Automatica 129 (2021) 109637

Contents lists available at ScienceDirect

Automatica

journal homepage: www.elsevier.com/locate/automatica

Adaptive event-triggered PDE control for load-moving cable systems ☆

Ji Wang *, Miroslav Krstic

Department of Mechanical and Aerospace Engineering, University of California, San Diego, La Jolla, CA 92093-0411, USA

ARTICLE INFO

Article history:
Received 7 April 2020
Received in revised form 23 November 2020
Accepted 7 March 2021
Available online 24 April 2021

Keywords:
Hyperbolic PDEs
Adaptive control
Backstepping
Event-triggered control
Cable elevators

ABSTRACT

Motivated by lateral vibration suppression of a mining cable elevator, which is a load-moving cable system, where the load moves along a viscoelastic guideway whose stiffness and damping coefficients are unknown, we present event-triggered adaptive output-feedback boundary control design of a hyperbolic PDE–ODE coupled system using the measurements at the PDE actuated boundary and the ODE, where the PDE subsystem is a class of 2×2 coupled hyperbolic PDEs with spatially-varying coefficients and on a time-varying domain, and a high uncertainty exist in the system matrix of the ODE subsystem at the uncontrolled boundary of the PDE. A continuous-in-time observer-based adaptive backstepping control law is designed where the control gains can be self-tuned to adjust the system matrix of the ODE into a given target system matrix, based on which an observer-based dynamic event-triggering mechanism is built and the existence of a minimal dwell-time is proved. The asymptotic stability of the overall adaptive event-based output-feedback closed-loop system is proved via Lyapunov analysis. In numerical simulation, the performance of the proposed controller is verified in lateral vibration suppression of a mining cable elevator.

© 2021 Elsevier Ltd. All rights reserved.

1. Introduction

1.1. Background

A load-moving cable system represents the prominent characteristic of a mining cable elevator which is used to transport a cage loaded with the minerals and miners between thousands of meters underground and the surface via cables (Kaczmarczyk & Ostachowicz, 2003). The undesirable mechanical vibrations are often caused in the high-speed moving, because of the stretching and contracting abilities of cables (Wang, Koga, Pi, & Krstic, 2018). It would not only increase the risk of cable fracture but also cause discomfort or injury to miners. Active vibration control is one economic way to suppress the vibrations because the main structure of the cable mining elevator does not need to be changed.

Cable is one of the typical flexible mechanical structures which are described by distributed parameter systems. Some PDE boundary control strategies have been proposed to suppress the vibrations in the flexible structures via boundary actuation. An iterative learning control scheme was proposed for some flexible structures under spatiotemporally varying disturbances in He, Meng, He, and Ge (2018). Boundary control to dampen the oscillations of a disturbed flexible string system was proposed in Zhao, Ahn, and Li (2019). A boundary control strategy was designed to suppress the bending and twisting vibrations of the rigid–flexible wing system in He, Wang, He, Yang, and Kaynak (2020). Two boundary controllers were designed to restrain the vibrations of a floating wind turbine connected with two flexible mooring lines in He, Xiang, He, and Li (2020). A boundary control law was presented to dampen the vibrations of a flexible hose used for aerial refueling in Liu, He, Zhao, Ahn, and Li (2020). Robust adaptive vibration control of uncertain spatial flexible riser systems with dead zone compensation was designed in Zhao, Ahn, and Li (2020).

The vibration dynamics of the cable is originally described by a second-order hyperbolic PDE, which can be converted into a class of coupled transport PDEs (Auriol, Aarsnes, Martin, & Di Meglio, 2018; Coron, Vazquez, Krstic, & Bastin, 2013; Deutscher, 2017a, 2017b; Hu, Di Meglio, Vazquez, & Krstic, 2016; Vazquez, Krstic, & Coron, 2011) in Riemann coordinates (Wang, Pi, & Krstic, 2018). For the load-moving cable system, the dynamics are modeled by time-varying-domain coupled transport PDEs coupled with an ODE at the uncontrolled boundary, where the PDE describes the vibration dynamics of the cable of time-varying length and the ODE models the lumped parameter dynamics of the payload (cage), and the coupling between the PDE and the ODE is related to the kinematics and dynamics relationship between the cable and payload. Based on such a distributed parameter system,

☆ This work was supported by the National Science Foundation under Grants 1935329 and 1823983. The material in this paper was not presented at any conference. This paper was recommended for publication in revised form by Associate Editor James Lam under the direction of Editor Ian R. Petersen.

* Corresponding author.
E-mail addresses: jiw248@eng.ucsd.edu (J. Wang), krstic@ucsd.edu (M. Krstic).

https://doi.org/10.1016/j.automatica.2021.109637
0005-1098/© 2021 Elsevier Ltd. All rights reserved.

boundary control strategy was proposed to suppress the axial vibrations of a mining cable elevator in Wang, Pi, and Krstic (2018). For the lateral vibrations in the mining cable elevator, a different excitation source is interaction between the cage and the flexible guides (Wang, Pi, Hu, & Gong, 2017). The elastic support of flexible guides was approximate as a spring–damping system, i.e., a viscoelastic guide, in Terumichi, Ohtsuka, and Yoshizawa (1997) and Zhu and Xu (2003), where the equivalent stiffness and damping coefficients are difficult to be known exactly. It leads to uncertainties existing in the parameters of the system matrix of the ODE describing the cage dynamics.

1.2. Adaptive boundary control of coupled hyperbolic PDEs

Adaptive strategies are widely used in control of various types of PDEs with unknown system parameters, including the considered coupled hyperbolic PDEs. In Anfinsen and Aamo (2017) an adaptive boundary control design of coupled hyperbolic PDEs with uncertain boundary and spatially-varying in-domain coefficients was presented. In Anfinsen and Aamo (2018), two adaptive boundary controllers of coupled hyperbolic PDEs with unknown in-domain and boundary parameters were proposed using identifier and swapping design respectively. Adaptive boundary control of a hyperbolic PDE–ODE coupled system, where the unknown parameters exist in the ODE, was considered in Wang, Tang, and Krstic (2020a, 2020b). It is worth reminding that in vibration control of a compliant mechanism whose first-order nature frequency is low, such as the cable system, the transient of adaptive learning in the control input may arouse undesired vibrations, even resonance.

1.3. Sampling scheme in PDE control

A new adaptive estimation with sampling update instants consisting of a least-square identifier and regulation triggers is proposed for parabolic PDEs (Karafyllis, Krstic, & Chrysafi, 2019), developed from ODE cases (Karafyllis, Kontorinaki, & Krstic, 2019; Karafyllis & Krstic, 2018b). It has advantages of guaranteeing exponential convergence of the state to zero, finite-time convergence of the estimate to the true value, and allowing using the certainty-equivalence approach. The resulting adaptive certainty-equivalence controller consists of sampling adaptive estimates and continuous plant states, i.e., the triggers only staying in the adaptive update law. Even though it can release the adaptive learning transient problem mentioned above, the use of the continuous states, i.e., vibration states of the cable, in the control law makes it unsuitable for the mining cable elevator, because the hydraulic actuator (head sheaves and hydraulic cylinders) in the elevator is massive and barely keeps up with the control law with high-frequency vibration states.

Some sampling schemes applied in the control input are potential solutions to the above problem. Designs of sampled-data control inputs of parabolic PDEs were presented in Fridman and Blighovsky (2012), Karafyllis and Krstic (2018a), and those of hyperbolic PDEs were proposed in Davo, Bresch-Pietri, Prieur, and Di Meglio (2018) and Karafyllis and Krstic (2017). Compared with the periodic sampled-data control which may generate unnecessary actions of the massive actuator, event-triggered control, where the input of the massive actuator is only changed at the necessary times which are determined by an event-triggering mechanism of evaluating the operation of the elevator, is more feasible for the mining cable elevator, from the point of view of energy saving.

Most of current designs of event-triggering mechanisms (ETMs) are for ODE systems, such as Girard (2015), Marchand, Durand, and Castellanos (2013), Seuret, Prieur, and Marchand (2014) and Tabuada (2007). There are few studies about event-based control of PDE systems. Selivanov and Fridman (2016) and Yao and El-Farra (2013) proposed event-triggered control schemes for distributed (in-domain) control of PDEs. For the boundary control of PDEs, an event-triggered control law was originally proposed in Espitia, Girard, Marchand, and Prieur (2016a, 2016b) for hyperbolic PDEs with dissipativity boundary conditions. Afterwards, event-triggered boundary control of a reaction–diffusion PDE was also proposed in Espitia, Karafyllis, and Krstic (2021). A state-feedback event-based boundary controller of 2×2 coupled linear hyperbolic PDEs was first proposed in Espitia, Girard, Marchand, and Prieur (2018), and the observer-based event-triggered boundary control of 2×2 coupled linear hyperbolic PDEs was in further developed in Espitia (2020). An event-triggered boundary control of 2×2 coupled hyperbolic PDEs sandwiched by two ODEs was proposed in Wang and Krstic (2021). However the above-mentioned results focus on a fixed-domain PDE with constant and completely known parameters, which is not suitable for the problem considered in this paper, especially the time-varying property of the PDE domain and the potential learning transition under the unknown parameters need to be in further considered in the event-based control system design.

1.4. Contributions

- Compared with Anfinsen and Aamo (2017), Anfinsen and Aamo (2018) and Anfinsen and Aamo (2019) about adaptive control of coupled hyperbolic PDEs in the continuous-in-time form, this paper proposes an event-triggered version of adaptive control of this kind of PDE system.
- As compared to Espitia (2020), Espitia et al. (2018) and Wang and Krstic (2021) which designed event-triggered backstepping control for 2×2 hyperbolic PDEs on a fixed-domain PDE with constant and completely known plant parameters, the time-varying domain and the spatially-varying coefficients in the 2×2 hyperbolic PDEs, and the highly uncertain ODE coupled at the uncontrolled PDE boundary, make the control design in this paper more challenging.
- This is the first result about adaptive event-triggered backstepping boundary control of coupled hyperbolic PDEs, with application into lateral vibration control of a mining cable elevator moving along viscoelastic guideways whose stiffness and damping coefficients are unknown.

1.5. Organization

The rest of the paper is organized as follows. The problem formulation is shown in Section 2. An observer is designed to estimate the PDE states in Section 3. The design of an observer-based adaptive backstepping controller is presented in Section 4. An observer-based event-triggering mechanism and the proof of the existence of a minimal dwell-time are presented in Section 5. The stability of the resulting adaptive event-based closed-loop control system is proved in Section 6. Simulation test in a mining cable elevator model is conducted in Section 7. The conclusion and future work are presented in Section 8.

Notation. Throughout this paper, the partial derivatives and total derivatives are denoted as: $f_x(x,t) = \frac{\partial f}{\partial x}(x,t)$, $f_t(x,t) = \frac{\partial f}{\partial t}(x,t)$, $f'(x) = \frac{df(x)}{dx}$, $\dot{f}(t) = \frac{df(t)}{dt}$.

2. Problem formulation

The load-moving cable is originally modeled by a wave PDE–ODE system on a time-varying domain (Wang, Koga, et al., 2018; Wang, Tang, Pi, & Krstic, 2018), which can be rewritten as a 2×2 coupled transport PDE–ODE system on a time-varying domain in the Riemann coordinates (Wang, Pi, & Krstic, 2018). Our control design is based on a general 2×2 coupled transport PDE–ODE system with spatially-varying coefficients and on a time-varying domain, and the application into vibration control of a mining cable elevator, which is a representative of the load-moving cable system, will be conducted in Section 7, where the physical meanings of the considered PDE plant will be presented.

The general plant considered in this paper is

$$\dot{X}(t) = AX(t) + Bw(0,t), \tag{1}$$

$$z(0,t) = CX(t) + p_1 w(0,t), \tag{2}$$

$$z_t(x,t) = -q_1(x)z_x(x,t) + c_1(x)z(x,t) + c_2(x)w(x,t), \tag{3}$$

$$w_t(x,t) = q_2(x)w_x(x,t) + c_3(x)z(x,t) + c_4(x)w(x,t), \tag{4}$$

$$w(l(t),t) = U(t), \tag{5}$$

with $x \in [0, l(t)], t \in [0,\infty)$. The vector $X(t) \in R^n$ is an ODE state and the scalars $z(x,t)$, $w(x,t)$ are PDE states. Eq. (5) is the boundary condition with control input $U(t)$ to be designed, which represents the boundary control force for vibration suppression in a load-moving cable system. There always exists another control input for moving regulation in the load-moving cable system, which is not the design task in this paper, and the proximal reflection term arising from converting the wave PDE to the 2×2 coupled transport PDE is considered as compensated by this motion regulation control input. For the example of the mining cable elevator in the simulation, the proximal reflection term $z(l(t),t)$ is compensated by the motion regulation control force at the drum (see Figure 1 (a) in Wang, Koga, et al. (2018)), and the control design in this paper acts as a vibration control force applied at the head sheave.

Spatially-varying transport speeds $q_1(x), q_2(x) \in C^1$ are positive and $c_1(x), c_2(x), c_3(x), c_4(x) \in C^0$ are arbitrary. The constant p_1 is nonzero. The matrix $C \in R^{1\times n}$ is arbitrary. The input matrix $B \in R^{n\times 1}$ and the system matrix $A \in R^{n\times n}$ with unknown parameters satisfy the following assumptions.

Assumption 1. The matrices A, B are in the form of

$$A = \begin{pmatrix} 0 & 1 & 0 & 0 & \cdots & 0 \\ 0 & 0 & 1 & 0 & \cdots & 0 \\ & & \vdots & & & \\ 0 & 0 & 0 & 0 & \cdots & 1 \\ g_1 & g_2 & g_3 & \cdots & g_{n-1} & g_n \end{pmatrix}, B = \begin{pmatrix} 0 \\ 0 \\ 0 \\ 0 \\ h_n \end{pmatrix} \tag{6}$$

where the constants $g_1, g_2, g_3, \ldots, g_{n-1}, g_n$ are unknown and arbitrary, and their lower and upper bounds are known and arbitrary. The constant h_n is nonzero and known.

Assumption 1 indicates that the ODE is in the controllable form, which covers many practical models, including the payload dynamics in the load-moving cable systems.

Choose a target Hurwitz matrix

$$A_m = \begin{pmatrix} 0 & 1 & 0 & 0 & \cdots & 0 \\ 0 & 0 & 1 & 0 & \cdots & 0 \\ & & \vdots & & & \\ 0 & 0 & 0 & 0 & \cdots & 1 \\ \bar{g}_1 & \bar{g}_2 & \bar{g}_3 & \cdots & \bar{g}_{n-1} & \bar{g}_n \end{pmatrix} \tag{7}$$

where the coefficients $\bar{g}_1, \bar{g}_2, \bar{g}_3, \ldots, \bar{g}_{n-1}, \bar{g}_n$ are determined by the user according to the desired performance for the specific application.

According to Assumption 1 and (7), we know that there exists a unique, though unknown, row vector

$$K_{1\times n} = [k_1, \ldots, k_n] \tag{8}$$

such that

$$A_m = A + BK \tag{9}$$

and

$$\bar{g}_i = g_i + h_n k_i, \quad i = 1, 2, \ldots, n. \tag{10}$$

By virtue of (10), while the k_i's are unknown, the lower and upper bounds on the k_i's, i.e., $[\underline{k}_i, \bar{k}_i]$, $i = 1, 2, \ldots, n$ are known because the lower and upper bounds of the system matrix coefficients g_i's are known in Assumption 1, and the target matrix coefficients $\bar{g}_i$'s are chosen by the user.

The time-varying domain, i.e., the moving boundary $l(t)$ is under the following two assumptions.

Assumption 2. The function $l(t)$ is uniformly bounded, i.e., $0 < l(t) \le L, \forall t \ge 0$, where L is a positive constant.

Assumption 3. The function $\dot{l}(t)$ is bounded as

$$|\dot{l}(t)| \le v_m < \min_{0\le x\le L}\{q_1(x), q_2(x)\}, \tag{11}$$

where v_m is the maximum velocity of the moving boundary.

The limit of the speed of the moving boundary in Assumption 3 is to ensure the well-posedness of the plant (1)–(5) according to Gugat (2007a, 2007b).

The complete set of the plant parameters is given by

$$\zeta_p = \{p_1, q_1, q_2, c_1, c_2, c_3, c_4, A, B, L, v_m\}, \tag{12}$$

where x is omitted for conciseness.

3. Observer

To estimate the PDE states $z(x,t)$, $w(x,t)$, which usually cannot be fully measured in practice but are employed in the controller, an observer using the measurements $X(t)$, $z(l(t),t)$ is formulated as

$$\dot{X}(t) = AX(t) + B\hat{w}(0,t) + B\tilde{w}(0,t), \tag{13}$$

$$\hat{z}(0,t) = CX(t) + p_1\hat{w}(0,t), \tag{14}$$

$$\begin{aligned}\hat{z}_t(x,t) =& -q_1(x)\hat{z}_x(x,t) + c_1(x)\hat{z}(x,t) + c_2(x)\hat{w}(x,t) \\ &+ \Psi_2(x,l(t))(z(l(t),t) - \hat{z}(l(t),t)),\end{aligned} \tag{15}$$

$$\begin{aligned}\hat{w}_t(x,t) =& q_2(x)\hat{w}_x(x,t) + c_3(x)\hat{z}(x,t) + c_4(x)\hat{w}(x,t) \\ &+ \Psi_3(x,l(t))(z(l(t),t) - \hat{z}(l(t),t)),\end{aligned} \tag{16}$$

$$\hat{w}(l(t),t) = U(t), \tag{17}$$

where (13) is exactly the ODE (1) with $w(0,t) = \hat{w}(0,t) + \tilde{w}(0,t)$, providing the measured signal $X(t)$ into (14). It should be noted that (13) is not computed online as a part of the observer. The observer gains $\Psi_2(x,l(t))$, $\Psi_3(x,l(t))$ are to be determined. As we indicate, because the ODE state X is available, the observer (14)–(17) is only to estimate the PDE states. Let us denote the observer error states as

$$(\tilde{z}(x,t), \tilde{w}(x,t)) = (z(x,t), w(x,t)) - (\hat{z}(x,t), \hat{w}(x,t)). \tag{18}$$

According to (2)–(5) and (14)–(17), the observer error system is obtained as

$$\tilde{z}(0,t) = p_1\tilde{w}(0,t), \tag{19}$$

$$\begin{aligned}\tilde{z}_t(x,t) =& -q_1(x)\tilde{z}_x(x,t) + c_1(x)\tilde{z}(x,t) + c_2(x)\tilde{w}(x,t) \\ &- \Psi_2(x,l(t))\tilde{z}(l(t),t),\end{aligned} \tag{20}$$

$$\tilde{w}_t(x,t) = q_2(x)\tilde{w}_x(x,t) + c_3(x)\tilde{z}(x,t) + c_4(x)\tilde{w}(x,t) - \Psi_3(x,l(t))\tilde{z}(l(t),t), \tag{21}$$

$$\tilde{w}(l(t),t) = 0. \tag{22}$$

The observer gains $\Psi_2(x,l(t))$, $\Psi_3(x,l(t))$ are to be designed to ensure convergence to zero of the observer errors defined in (18). Next, we postulate the backstepping transformation

$$\tilde{z}(x,t) = \tilde{\alpha}(x,t) - \int_x^{l(t)} \bar{\phi}(x,y)\tilde{\alpha}(y,t)dy - \int_x^{l(t)} \check{\phi}(x,y)\tilde{\beta}(y,t)dy, \tag{23}$$

$$\tilde{w}(x,t) = \tilde{\beta}(x,t) - \int_x^{l(t)} \bar{\psi}(x,y)\tilde{\alpha}(y,t)dy - \int_x^{l(t)} \check{\psi}(x,y)\tilde{\beta}(y,t)dy \tag{24}$$

to convert the original observer error system (19)–(22) to the following target observer error system:

$$\tilde{\alpha}(0,t) = p_1\tilde{\beta}(0,t), \tag{25}$$

$$\tilde{\alpha}_t(x,t) = -q_1(x)\tilde{\alpha}_x(x,t) + c_1(x)\tilde{\alpha}(x,t), \tag{26}$$

$$\tilde{\beta}_t(x,t) = q_2(x)\tilde{\beta}_x(x,t) + c_4(x)\tilde{\beta}(x,t), \tag{27}$$

$$\tilde{\beta}(l(t),t) = 0. \tag{28}$$

Even though the integration interval $[0, l(t)]$ is time-varying, the kernels in (23), (24) need not include the argument $l(t)$ because the extra terms in which $l(t)$, $\dot{l}(t)$ appear in the course of calculating the kernel conditions will be "absorbed" by the observer gains $\Psi_2(x,l(t))$, $\Psi_3(x,l(t))$. By matching (19)–(22) and (25)–(28) via (23), (24), we obtain PDE conditions on the kernels $\bar{\phi}(x,y)$, $\check{\phi}(x,y)$, $\bar{\psi}(x,y)$, $\check{\psi}(x,y)$, as follows,

$$\bar{\psi}(x,x) = \frac{-c_3(x)}{q_1(x)+q_2(x)}, \bar{\phi}(0,y) = p_1\bar{\psi}(0,y), \tag{29}$$

$$-q_1(y)\bar{\psi}_y(x,y) + q_2(x)\bar{\psi}_x(x,y) + c_3(x)\bar{\phi}(x,y) + (c_4(x) - c_1(y) - q_1'(y))\bar{\psi}(x,y) = 0, \tag{30}$$

$$-q_1(x)\bar{\phi}_x(x,y) - q_1(y)\bar{\phi}_y(x,y) + (c_1(x) - c_1(y) - q_1'(y))\bar{\phi}(x,y) + c_2(x)\bar{\psi}(x,y) = 0, \tag{31}$$

$$q_2(y)\check{\phi}_y(x,y) - q_1(x)\check{\phi}_x(x,y) + (c_1(x) - c_4(y) + q_2'(y))\check{\phi}(x,y) + c_2(x)\check{\psi}(x,y) = 0, \tag{32}$$

$$q_2(x)\check{\psi}_x(x,y) + q_2(y)\check{\psi}_y(x,y) + c_3(x)\check{\phi}(x,y) + (c_4(x) - c_4(y) + q_2'(y))\check{\psi}(x,y) = 0, \tag{33}$$

$$\check{\psi}(0,y) = \frac{1}{p_1}\check{\phi}(0,y), \check{\phi}(x,x) = \frac{c_2(x)}{q_1(x)+q_2(x)}. \tag{34}$$

The equation set (29)–(34) is well-posed because they belong to a general class of kernel equations whose well-posedness is proved in Theorem 3.2 of Di Meglio, Bribiesca, Hu, and Krstic (2018). Then the observer gains are then deduced as

$$\Psi_2(x,l(t)) = \dot{l}(t)\bar{\phi}(x,l(t)) - q_1(l(t))\bar{\phi}(x,l(t)), \tag{35}$$

$$\Psi_3(x,l(t)) = \dot{l}(t)\bar{\psi}(x,l(t)) - q_1(l(t))\bar{\psi}(x,l(t)). \tag{36}$$

Lemma 1. *For the observer error system (19)–(22), the state estimation errors $\tilde{z}(x,t)$, $\tilde{w}(x,t)$ become zero after $t_f = \frac{L}{\min_{0\le x\le L}\{q_1(x)\}} + \frac{L}{\min_{0\le x\le L}\{q_2(x)\}}$.*

Proof. According to the target observer error system (25)–(28) and the result in Hu et al. (2016), we know that $\tilde{\alpha}(x,t)$, $\tilde{\beta}(x,t)$ become zero after the finite time t_f. Applying the Cauchy–Schwarz inequality into (23), (24), the proof of this lemma is complete. ■

The finite time in which Lemma 1 establishes that the observer errors vanish is only dependent on the plant parameters and not on the controller parameters. In the next section, we first design a continuous-in-time adaptive control law to stabilize the coupled transport PDEs coupled with a highly uncertain ODE at the uncontrolled boundary. Then we design an event-triggering mechanism, which uses the signals from the observer and includes an internal dynamic variable and which produces triggering times based on evaluating the size of the deviation of the control input applied over the interval between the triggers from the continuous-in-time control signal. The combined continuous-in-time adaptive controller and the event-triggering mechanism constitute the adaptive event-triggered boundary controller.

4. Adaptive continuous-in-time control design

In this section, we conduct a state-feedback control backstepping design, with the intent of feeding into this full-state designs the observer states from the observer in the previous section. In other words, in this section we design an observer-based output-feedback controller which we then make adaptive. The output error injections $\tilde{z}(l(t),t)$, $\tilde{w}(0,t)$ in the observer are regarded as zero in the state-feedback design, and then the separation principle, which is verified by the fact that the stability of the observer error system is independent of the control design according to Lemma 1, is applied in the stability analysis of the resulting closed-loop system.

4.1. Backstepping

Two transformations are used to convert (13)–(17) to a target system, with purposes of removing the couplings in the PDE domain and making the ODE system matrix Hurwitz.

(a) The first transformation to decouple PDEs

We postulate the backstepping transformation

$$\hat{\alpha}(x,t) = \hat{z}(x,t) - \int_0^x J(x,y)\hat{z}(y,t)dy - \int_0^x G(x,y)\hat{w}(y,t)dy, \tag{37}$$

$$\hat{\beta}(x,t) = \hat{w}(x,t) - \int_0^x F(x,y)\hat{z}(y,t)dy - \int_0^x N(x,y)\hat{w}(y,t)dy, \tag{38}$$

to convert (13)–(17) to the following system

$$\dot{X}(t) = AX(t) + B\hat{\beta}(0,t), \tag{39}$$

$$\hat{\alpha}(0,t) = CX(t) + p_1\hat{\beta}(0,t), \tag{40}$$

$$\hat{\alpha}_t(x,t) = -q_1(x)\hat{\alpha}_x(x,t) + c_1(x)\hat{\alpha}(x,t) - J(x,0)q_1(0)CX(t), \tag{41}$$

$$\hat{\beta}_t(x,t) = q_2(x)\hat{\beta}_x(x,t) + c_4(x)\hat{\beta}(x,t) - F(x,0)q_1(0)CX(t), \tag{42}$$

$$\hat{\beta}(l(t),t) = U(t) - \int_0^{l(t)} F(l(t),y)\hat{z}(y,t)dy - \int_0^{l(t)} N(l(t),y)\hat{w}(y,t)dy. \tag{43}$$

By matching (39)–(43) with (13)–(17) via (37), (38), we obtain the conditions of the kernels $J(x,y)G(x,y)F(x,y)N(x,y)$, as follows,

$$G(x,x) = \frac{c_2(x)}{q_1(x)+q_2(x)}, J(x,0) = G(x,0)\frac{q_2(0)}{q_1(0)p_1}, \tag{44}$$

$$q_2(y)G_y(x,y) - q_1(x)G_x(x,y) - c_2(y)J(x,y) + (c_1(x) - c_4(y) + q_2'(y))G(x,y) = 0, \tag{45}$$

$$q_1(y)J_y(x,y) + q_1(x)J_x(x,y)$$

$$+\ c_3(y)G(x,y)+(c_1(y)-c_1(x)+q_1{}'(y))J(x,y)=0, \tag{46}$$

$$F(x,x)=\frac{-c_3(x)}{q_1(x)+q_2(x)},\ N(x,0)=F(x,0)\frac{q_1(0)p_1}{q_2(0)}, \tag{47}$$

$$q_2(y)N_y(x,y)+q_2(x)N_x(x,y)$$
$$-\ c_2(y)F(x,y)+(c_4(x)-c_4(y)+q_2{}'(y))N(x,y)=0, \tag{48}$$

$$q_1(y)F_y(x,y)-q_2(x)F_x(x,y)$$
$$+\ c_3(y)N(x,y)+(c_1(y)-c_4(x)+q_1{}'(y))F(x,y)=0, \tag{49}$$

which is a special case of (60)–(73) in Wang and Krstic (2020) where (61) and (68) in Wang and Krstic (2020) hold naturally here because the PDE states are scalar in this paper. Please refer to Lemma 1 in Wang and Krstic (2020) for the well-posedness of (44)–(49).

(b) The second transformation to form a stable ODE

We postulate the backstepping transformation

$$\hat\eta(x,t)=\hat\beta(x,t)-\int_0^x\hat N(x,y;\hat K(t))\hat\beta(y,t)dy-D(x;\hat K(t))X(t) \tag{50}$$

where $\hat K(t)\in R^{1\times n}$ is the estimate of the ideal control gains and will be shown later. The conditions on the kernels $\hat N(x,y;\hat K(t))$, $D(x;\hat K(t))$ are to be determined next. The inverse transformation is postulated as

$$\hat\beta(x,t)=\hat\eta(x,t)-\int_0^x\hat N_I(x,y;\hat K(t))\hat\eta(y,t)dy-D_I(x;\hat K(t))X(t) \tag{51}$$

where $\hat N_I(x,y;\hat K(t))$, $D_I(x;\hat K(t))$ are kernels which can be determined after the determination of $\hat N(x,y;\hat K(t))$, $D(x;\hat K(t))$.

Through the transformation (50), we convert (39)–(43) into the following target system:

$$\dot X(t)=A_mX(t)-B\tilde K(t)X(t)+B\hat\eta(0,t), \tag{52}$$

$$\hat\alpha(0,t)=(C+p_1D(0;\hat K(t)))X(t)+p_1\hat\eta(0,t), \tag{53}$$

$$\hat\alpha_t(x,t)=-q_1(x)\hat\alpha_x(x,t)+c_1(x)\hat\alpha(x,t)-J(x,0)q_1(0)CX(t), \tag{54}$$

$$\hat\eta_t(x,t)=q_2(x)\hat\eta_x(x,t)+c_4(x)\hat\eta(x,t)-\dot{\hat K}(t)R(x,t)$$
$$+\ \left(D(x;\hat K(t))B\tilde K(t)-\dot{\hat K}(t)D_{\hat K(t)}(x;\hat K(t))\right)X(t), \tag{55}$$

$$\hat\eta(l(t),t)=0, \tag{56}$$

where

$$\tilde K(t)=K-\hat K(t), \tag{57}$$

and where

$$R(x,t)=\int_0^x\hat N_{\hat K(t)}(x,y;\hat K(t))\hat\beta(y,t)dy$$
$$=\int_0^x\hat N_{\hat K(t)}(x,y;\hat K(t))\left[\hat\eta(y,t)-\int_0^y\hat N_I(y,\sigma;\hat K(t))\hat\eta(\sigma,t)d\sigma\right.$$
$$\left.-\ D_I(y;\hat K(t))X(t)\right]dy. \tag{58}$$

The partial derivatives appearing in (55)–(58), respectively, are $D_{\hat K(t)}(x;\hat K(t))=\frac{\partial D(x;\hat K(t))}{\partial\hat K(t)}$ and $\hat N_{\hat K(t)}(x,y;\hat K(t))=\frac{\partial\hat N(x,y;\hat K(t))}{\partial\hat K(t)}$. By matching (39)–(43) and (52)–(56) via (50), the conditions of the kernels $N(x,y;\hat K(t))$, $D(x;\hat K(t))$ in (50) are determined as

$$D(0;\hat K(t))=\hat K(t), \tag{59}$$

$$-q_2(x)D'(x;\hat K(t))+D(x;\hat K(t))(A_m-c_4(x)-B\hat K(t))$$
$$+\ F(x,0)q_1(0)C-\int_0^x\hat N(x,y;\hat K(t))F(y,0)q_1(0)Cdy=0, \tag{60}$$

$$q_2(y)\hat N_y(x,y;\hat K(t))$$
$$+\ q_2(x)\hat N_x(x,y;\hat K(t))+q_2{}'(y)\hat N(x,y;\hat K(t))=0, \tag{61}$$

$$q_2(0)\hat N(x,0;\hat K(t))=D(x;\hat K(t))B. \tag{62}$$

The equation set (59)–(62) is a transport PDE–ODE coupled system consisting of the transport PDE (61) with the boundary condition (62) on $\{(x,y)|0\le y\le x\le l(t)\}$ and the ODE (60) with the initial value (59) on $\{0\le x\le l(t)\}$. It should be noted that $\hat K(t)$ is a parameter rather than a variable in the transport PDE (61), (62) with respect to the independent variables x,y and in the ODE (59), (60) with respect to the independent variable x. In the study of well-posedness of (59)–(62), the transport PDE state $\hat N(x,y;\hat K(t))$ can be represented by its boundary value $D(x;\hat K(t))B$. Substituting the result into ODE (60) to replace $\hat N(x,y;\hat K(t))$, the unique and continuous solution of the first-order ODE $\hat D(x;\hat K(t))$ (60) can be obtained. Then the unique and continuous solution of the transport PDE $\hat N(x,y;\hat K(t))$ in (61), (62) is obtained because of the well-defined and continuous input signal in (62). Following Section 2.4 in Wang, Krstic, and Pi (2018), the kernels $\hat N_I(x,y;\hat K(t))$, $D_I(x;\hat K(t))$ in the inverse transformation can then be determined.

4.2. Adaptive update laws

The objective in this section is to build adaptive update laws to obtain self-tuning of the control gains $\hat K(t)=[\hat k_1(t),\dots,\hat k_n(t)]$, where normalization and projection operators are used to guarantee boundedness, as is typical in adaptive control designs. The adaptive update law $\hat K(t)=[\hat k_1,\dots,\hat k_n]$ is of the form

$$\dot{\hat k}_i(t)=\mathrm{Proj}_{[\underline k_i,\bar k_i]}\left(\tau_i(t),\hat k_i(t)\right). \tag{63}$$

While projection is applicable for arbitrary convex sets, the set within which the control gain vector K should reside in a hyperrectangle or, as is colloquially said, the estimate $\hat K(t)$ should be maintained within box constraints. Given the hyperrectangular set for the feedback gains, for any $m\le M$ and any r,p, $\mathrm{Proj}_{[m,M]}$ is defined as the operator given by

$$\mathrm{Proj}_{[m,M]}(r,p)=\begin{cases}0, & \text{if } p=m \text{ and } r<0,\\ 0, & \text{if } p=M \text{ and } r>0,\\ r, & \text{else.}\end{cases}$$

So, the projection operator is to keep the scalar components of parameter estimate vector $\hat K(t)=[\hat k_1,\dots,\hat k_n]$ bounded within the interval $[\underline k_i,\bar k_i]$. The bounds $\underline k_i$ and $\bar k_i$ are determined from the bounds on the unknown parameters in A using Assumption 1, as well as (7) and (10). We choose the parameter update rate functions τ_i in (63) as

$$[\tau_1(t),\dots,\tau_n(t)]^T=\frac{\Gamma_c}{1+\Omega(t)-\mu_m m_d(t)}\left[-2X(t)B^TPX(t)\right.$$
$$\left.+\ r_a\int_0^{l(t)}e^{\delta x}\hat\eta(x,t)X(t)B^TD(x;\hat K(t))^Tdx\right], \tag{64}$$

where $m_d(t)<0$, a dynamic variable in the event-triggering mechanism, will be defined in next section, and the adaptation gain matrix is

$$\Gamma_c=\mathrm{diag}\{\gamma_{c1},\dots,\gamma_{cn}\}, \tag{65}$$

and where $\Omega(t)$ is defined as

$$\Omega(t)=X(t)^TPX(t)+\frac12r_a\int_0^{l(t)}e^{\delta x}\hat\eta(x,t)^2dx$$
$$+\ \frac12r_b\int_0^{l(t)}e^{-\delta x}\hat\alpha(x,t)^2dx. \tag{66}$$

The determination of the positive constants δ, r_a and r_b will be shown in the next section. The matrix $P = P^T > 0$ is the unique solution to the Lyapunov equation

$$PA_m + A_m^T P = -Q \tag{67}$$

for some $Q = Q^T > 0$. It should be noted that P is known since A_m is known (chosen by the user). We introduce the normalization $\Omega(t) + 1$ in the denominator in (64) in order to keep the rate of change of the parameter estimate $\hat{\hat{K}}(t)$ bounded, which will be used in estimating a minimal dwell-time in ETM and the stability analysis of the closed-loop system. The functions $\hat{\eta}(x,t)$ and $\hat{\alpha}(x,t)$ in (64)–(66) can be represented by the observer states through (37), (38), (50). The complete set of positive design parameters in the parameter update law is defined as

$$\zeta_a = \{\Gamma_c, \delta, r_a, r_b, \mu_m\}. \tag{68}$$

The update law designs in this section will be chosen with the help of a Lyapunov analysis in Section 6.

4.3. Continuous-in-time control law

The continuous-in-time adaptive backstepping control law is derived in this section. For (56) to hold, using (43), recalling (38), (50), we get

$$\begin{aligned} U(t) = &\int_0^{l(t)} \bar{M}(l(t), x; \hat{K}(t))\hat{z}(x,t)dx + D(l(t); \hat{K}(t))X(t) \\ &+ \int_0^{l(t)} \bar{N}(l(t), x; \hat{K}(t))\hat{w}(x,t)dx \end{aligned} \tag{69}$$

where $\bar{M}(l(t), x; \hat{K}(t))$, $\bar{N}(l(t), x; \hat{K}(t))$ are

$$\bar{M}(l(t), x; \hat{K}(t)) = F(l(t), x) - \int_x^{l(t)} \hat{N}(l(t), y; \hat{K}(t))F(y, x)dy, \tag{70}$$

$$\begin{aligned} \bar{N}(l(t), x; \hat{K}(t)) = &N(l(t), x) + \hat{N}(l(t), x; \hat{K}(t)) \\ &- \int_x^{l(t)} \hat{N}(l(t), y; \hat{K}(t))N(y, x)dy. \end{aligned} \tag{71}$$

In the output-feedback adaptive backstepping control law (69), the states $\hat{w}(x,t)$, $\hat{z}(x,t)$ are from the observer (14)–(17). The kernels $J, F, G, N, \hat{N}, D$ are derived from the backstepping process in this section. The state $X(t)$ is the measurement. The row vector $\hat{K}(t)$ is the adaptive estimate defined in (63), (64).

5. Event-triggering mechanism

In this section, we introduce an observer-based event-triggered control scheme for stabilization of plant (1)–(5). It relies on both the continuous-in-time adaptive control signal $U(t)$ in (69) and a dynamic event-triggering mechanism (ETM) which determines triggering times t_k (integer $k \geq 0$ and $t_0 = 0$) when the control signal is updated, and between updates the control signal is held constant in a zero-order-hold (ZOH) fashion. In other words, the event-triggered control signal $U_d(t)$ is the frozen value of the continuous-in-time one $U(t)$ at the time instants t_k, i.e.,

$$U_d(t) = U(t_k), \qquad t \in [t_k, t_{k+1}). \tag{72}$$

Inserting $U_d(t)$ into (17), we obtain

$$\hat{w}(l(t), t) = U_d(t). \tag{73}$$

A deviation $d(t)$ between the continuous-in-time adaptive control signal and the event-based control signal is given as

$$d(t) = U(t) - U_d(t). \tag{74}$$

Then (73) can be written as

$$\hat{w}(l(t), t) = U(t) - d(t). \tag{75}$$

Recalling the backstepping transformations and designs of $U(t)$ in Section 4, the target system becomes (52)–(55) with the right boundary condition

$$\hat{\eta}(l(t), t) = -d(t). \tag{76}$$

The ETM to determine the triggering times of U_d is designed, as in Espitia et al. (2018), using the dynamic triggering condition

$$t_{k+1} = \inf\{t \in R^+ | t > t_k | d(t)^2 \geq \theta\Phi(t) - m_d(t)\}, \tag{77}$$

where the internal dynamic variable $m_d(t)$ satisfies the ordinary differential equation

$$\begin{aligned} \dot{m}_d(t) = &-\eta m_d(t) + \lambda_d d(t)^2 - \sigma\Phi(t) - \kappa_1\hat{\alpha}(l(t), t)^2 \\ &- \kappa_2\hat{\eta}(0,t)^2 - \kappa_3\hat{\alpha}(0,t)^2 \end{aligned} \tag{78}$$

whose initial condition $m_d(0)$ should be chosen negative, and which is driven by the norm

$$\Phi(t) = |X(t)|^2 + \|\hat{\eta}(\cdot, t)\|^2 + \|\hat{\alpha}(\cdot, t)\|^2. \tag{79}$$

The signals in (79) can be replaced by the observer states via (37), (38), (50). The complete set of event-triggering mechanism parameters is as

$$\zeta_e = \{\theta, \eta, \lambda_d, \sigma, \kappa_1, \kappa_2, \kappa_3\}. \tag{80}$$

These positive parameters are to be determined later.

The reason for introducing an internal dynamic variable $m_d(t)$ into the event-triggering condition (77) is that the changing rate $\dot{d}(t)$ of the deviation between $U(t)$ and $U_d(t)$, up on which the dwell-time relies, includes as the last three terms in (78), the boundary states $\hat{\alpha}(l(t), t)$ $\hat{\eta}(0,t)$, $\hat{\alpha}(0,t)$, whose integration should be incorporated into the event-triggering condition (77) to avoid the Zeno phenomenon. The internal dynamic variable $m_d(t)$ is kept negative by the choice of θ. The explanation in this paragraph formalized through the following three lemmas.

Lemma 2. *For $d(t)$ defined in (74), there exists a positive constant λ_a dependent only on the plant parameters ζ_p and the design parameters $\bar{g}_i$'s in A_m in (7), such that*

$$\begin{aligned} \dot{d}(t)^2 \leq &\lambda_a(\zeta_p, \bar{g}_i)\Big(d(t)^2 + \hat{\alpha}(l(t), t)^2 + \hat{\eta}(0,t)^2 + \hat{\alpha}(0,t)^2 \\ &+ m_3(\zeta_p, \zeta_a, \bar{g}_i)\|\hat{\alpha}(\cdot, t)\|^2 + m_3(\zeta_p, \zeta_a, \bar{g}_i)\|\hat{\eta}(\cdot, t)\|^2 \\ &+ m_3(\zeta_p, \zeta_a, \bar{g}_i)|X(t)|^2\Big) \end{aligned} \tag{81}$$

for $t \in (t_k, t_{k+1})$, where m_3 is a positive constant dependent only on the plant parameters ζ_p, the adaptive law parameters ζ_a, and the design parameters $\bar{g}_i$'s in A_m.

Proof. The proof is shown in Appendix A. ■

In the proof of Lemma 2 and the following text in this paper, a constant followed by $(\cdot)$ denotes a constant that depends only on the parameters in the parentheses. For conciseness, after the first appearance of the constant, $(\cdot)$ will be omitted when it is unnecessary.

Lemma 3. *Choosing*

$$\theta \leq \frac{\sigma}{\lambda_d}, \tag{82}$$

for the internal dynamic variable $m_d(t)$ defined in (78), it holds that $m_d(t) < 0$.

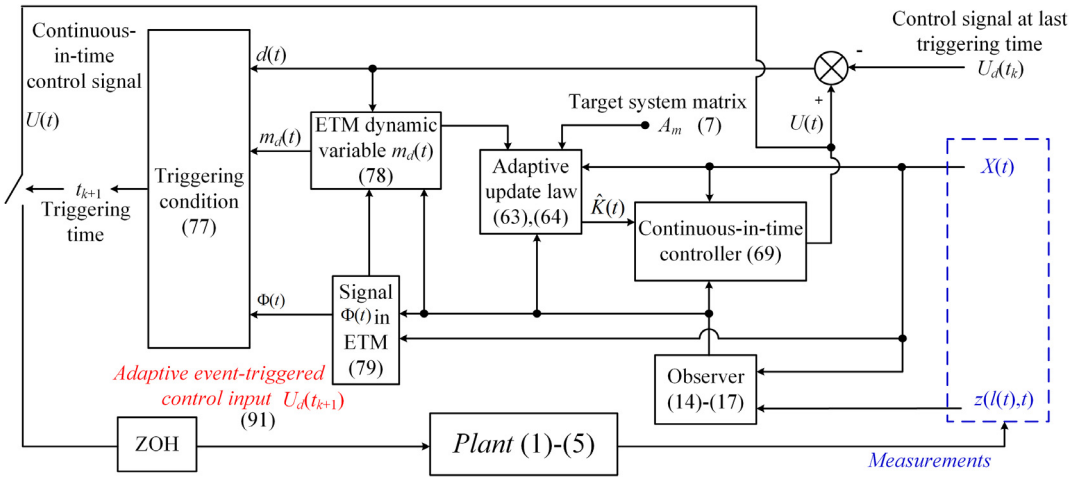

Fig. 1. Block of the event-based adaptive closed-loop control system.

Proof. The proof is shown in Appendix B. ■

Lemma 4. *For some $\kappa_1, \kappa_2, \kappa_3$, there exists a minimal dwell-time between two triggering times, which is equal to or greater than a positive constant $T_{\min}$, which depends only on the parameters of the plant and the choices of the design parameters.*

Proof. Introduce a function $\psi(t)$

$$\psi(t) = \frac{d(t)^2 + \frac{1}{2}m_d(t)}{\theta\Phi(t) - \frac{1}{2}m_d(t)} \tag{83}$$

which is proposed in Espitia et al. (2018). We have $\psi(t_{k+1}) = 1$ because the event condition in (77) is triggered, and $\psi(t_k) < 0$ because of $m_d(t) < 0$ (Lemma 3) and $d(t_k) = 0$. The function $\psi(t)$ is continuous on $[t_k, t_{k+1}]$ due to the continuity and well-posedness of this class of 2×2 hyperbolic PDE–ODE system according to Di Meglio et al. (2018). By the intermediate value theorem, there exists $t^* > t_k$ such that $\psi(t) \in [0, 1]$ when $t \in [t^*, t_{k+1}]$. The minimal $T_{\min}$ can be found as the minimal time it takes for $\psi(t)$ from 0 to 1, i.e., the reciprocal of the absolute value of the maximum changing rate of $\psi(t)$. Taking the derivative of (83), recalling Lemma 2, (78), (79), choosing

$$\kappa_1 \geq \max\{2\lambda_a(\zeta_p, \bar{g}_i), 2\theta\lambda_p(\zeta_p)\}, \tag{84}$$

$$\kappa_2 \geq \max\{2\lambda_a(\zeta_p, \bar{g}_i), 2\theta\lambda_p(\zeta_p)\}, \tag{85}$$

$$\kappa_3 \geq \max\{2\lambda_a(\zeta_p, \bar{g}_i), 2\theta\lambda_p(\zeta_p)\}, \tag{86}$$

for some positve λ_p given in Appendix C, through a calculation process shown in Appendix C, we get

$$\dot{\psi}(t) \leq n_1\psi(t)^2 + n_2\psi(t) + n_3 \tag{87}$$

with positive constants

$$n_1 = \frac{1}{2}\lambda_d + \theta\lambda_p(\zeta_p), \tag{88}$$

$$n_2 = 1 + \lambda_a(\zeta_p, \bar{g}_i) + \lambda_d + \theta\lambda_p(\zeta_p) + \eta + f_1(\sigma, \mu_0(\zeta_p, \zeta_a, \bar{g}_i), \theta), \tag{89}$$

$$n_3 = 1 + \frac{1}{2}\lambda_d + \lambda_a(\zeta_p, \bar{g}_i) + \frac{\lambda_a(\zeta_p, \bar{g}_i)m_3(\zeta_p, \zeta_a, \bar{g}_i)}{\theta} + \eta, \tag{90}$$

where the positive μ_0 only depends on the plant parameters, adaptive law parameters, and design parameters $\bar{g}_i$'s, and where

$$f_1 = \begin{cases} \mu_0(\zeta_p, \zeta_a, \bar{g}_i) - \frac{1}{2\theta}\sigma, & \text{if } \sigma < 2\theta\mu_0(\zeta_p, \zeta_a, \bar{g}_i), \\ 0, & \text{if } \sigma \geq 2\theta\mu_0(\zeta_p, \zeta_a, \bar{g}_i). \end{cases}$$

Then, it follows that the least time needed by $\psi(t)$ to go from 0 to 1 is

$$T_{\min} = \frac{1}{n_1 + n_2 + n_3} > 0,$$

because the maximum changing rate $\dot{\psi}(t)$ is $n_1 + n_2 + n_3$ for $\psi(t) \in [0, 1]$ according to (87). The proof of this lemma is complete. ■

6. Stability analysis of the closed-loop system

The expression of the final adaptive event-triggered control law U_d is

$$U_d(t) = \int_0^{l(t_k)} \bar{M}(l(t_k), x; \hat{K}(t_k))\hat{z}(x, t_k)dx + \int_0^{l(t_k)} \bar{N}(l(t_k), x; \hat{K}(t_k))\hat{w}(x, t_k)dx + D(l(t_k); \hat{K}(t_k))X(t_k) \tag{91}$$

for $t \in [t_k, t_{k+1})$, recalling (69) and (72). The triggering times t_k (for integer $k \geq 0$) are determined by the ETM in (77), (78). In (91), $\hat{z}$, $\hat{w}$ are states from the observer (14)–(17), $\hat{K}$ is the adaptive update law (63), (64), and X is the ODE measurement. The scalars $l(t_k)$ are the values of the time-varying function $l(t)$, which is known ahead of time, at the times t_k, the functions $\bar{M}$, $\bar{N}$ are given in (70), (71), and D is defined in (59)–(62). The block diagram of the event-based closed-loop system is shown in Fig. 1.

Lemma 5. *For all initial values $(\hat{\alpha}(\cdot, 0), \hat{\eta}(\cdot, 0)) \in L^2(0, L)$, $X(0) \in \mathbb{R}^n$, $m_d(0) < 0$, the event-based target system (52)–(55), (76) is asymptotically stable in the sense of* $\lim_{t\to\infty}(\|\hat{\alpha}(\cdot, t)\|^2 + \|\hat{\eta}(\cdot, t)\|^2 + |X(t)|^2 + |m_d(t)|) = 0$.

Proof. Define $\underline{q_1} = \min_{0\leq x\leq L}\{q_1(x)\}$, $\overline{q_1'} = \max_{0\leq x\leq L}\{|q_1'(x)|\}$, $\underline{q_2} = \min_{0\leq x\leq L}\{q_2(x)\}$, $\overline{q_2'} = \max_{0\leq x\leq L}\{|q_2'(x)|\}$, $\overline{q_1} = \max_{0\leq x\leq L}\{q_1(x)\}$, $\overline{q_2} = \max_{0\leq x\leq L}\{q_2(x)\}$, $\overline{c_1} = \max_{0\leq x\leq L}\{|c_1(x)|\}$, $\overline{c_4} = \max_{0\leq x\leq L}\{|c_4(x)|\}$.

Step 1: Choose the Lyapunov function as

$$V(t) = \ln(1 + \Omega(t) - \mu_m m_d(t)) + \frac{1}{2}\tilde{K}(t)\Gamma_c^{-1}\tilde{K}(t)^T \tag{92}$$

where the terms $\tilde{K}(t)$, $m_d(t)$ are related to the adaptive law and ETM. Because of $m_d(t) < 0$ (Lemma 3), we have that $1 + \Omega(t) - \mu_m m_d(t) > 0$. According to (66) and (79), we obtain

$$\mu_1\Phi(t) \leq \Omega(t) \leq \mu_2\Phi(t), \tag{93}$$

with positive μ_1, μ_2 as

$$\mu_1 = \frac{1}{2}\min\{r_a, r_b e^{-\delta L}, \lambda_{\min}(P)\}, \tag{94}$$

$$\mu_2 = \frac{1}{2}\max\{r_a e^{\delta L}, r_b, \lambda_{\max}(P)\}, \tag{95}$$

where $\lambda_{\min}$ and $\lambda_{\max}$ denote the minimum and maximum eigenvalues of the corresponding matrix. Taking the derivative of (92) along (52)–(55) with (76) and (78), and applying the Young and Cauchy–Schwarz inequalities, through a process in Appendix D, we arrive at

$$\begin{aligned}
\dot V(t) \le{}& \frac{1}{1+\Omega(t)-\mu_m m_d(t)}\Bigg[-\Bigg(\frac{7}{8}\lambda_{\min}(Q) - q_1(0) r_b \bar D^2 \\
&- \frac{1}{2} q_1(0)^2 L r_b \bar J^2 |C|^2 - \mu_m \sigma - \mu_m \kappa_3 \bar D^2\Bigg)|X(t)|^2 \\
&- \left(\frac{1}{2} q_2(0) r_a - (q_1(0) r_b + \mu_m \kappa_3) p_1^2 - \frac{8|PB|^2}{\lambda_{\min}(Q)} - \mu_m \kappa_2\right)\hat\eta(0,t)^2 \\
&- \left[r_a\left(\frac{1}{2}\delta \underline{q_2} - \overline{c_4} - \frac{1}{2}\overline{q_2'}\right)e^{\delta x} - \mu_m\sigma\right]\int_0^{l(t)} \hat\eta(x,t)^2 dx \\
&- \left[\frac{1}{2}(q_1(l(t)) - \dot l) r_b e^{-\delta l(t)} - \mu_m \kappa_1\right]\hat\alpha(l(t),t)^2 \\
&- \left[r_b\left(\frac{1}{2}\underline{q_1}\delta - \overline{c_1} - \frac{1}{2} - \frac{\overline{q_1'}}{2}\right)e^{-\delta x} - \mu_m\sigma\right]\int_0^{l(t)} \hat\alpha(x,t)^2 dx \\
&- r_a\int_0^{l(t)} e^{\delta x}\hat\eta(x,t)\Big(\dot{\hat K}(t) D_{\hat K(t)}(x;\hat K(t)) X(t) + \dot{\hat K}(t) R(x,t)\Big)dx \\
&- \left(\mu_m\lambda_d - \frac{1}{2}(\overline{q_2} + v_m) r_a e^{\delta L}\right) d(t)^2 + \mu_m \eta m_d(t)\Bigg]
\end{aligned} \tag{96}$$

where $\bar J = \max_{0\le x\le L}\{|J(x,0)|\}$, $\bar D = \max_{\underline{k}_i \le \hat k_i(t) \le \bar k_i}\{|C + p_1 D(0;\hat K(t))|\}$, and (76), (63), (64), (53) have been used.

Inserting (82) into (84)–(86) to replace θ by $\frac{\sigma}{\lambda_d}$, adding additional condition

$$\lambda_d \ge 1,$$

the conditions of the design parameters in adaptive event-triggered backstepping control systems are summarized as

$$\min\{\kappa_1, \kappa_2, \kappa_3\} \ge \max\{2\lambda_a, 2\sigma\lambda_p\}, \tag{97}$$

$$\delta > \max\left\{\frac{2\overline{c_4} + \overline{q_2'}}{\underline{q_2}}, \frac{2\overline{c_1} + 1 + \overline{q_1'}}{\underline{q_1}}\right\}, \tag{98}$$

$$r_b < \frac{\frac{7}{8}\lambda_{\min}(Q)}{q_1(0)\bar D^2 + \frac{1}{2} q_1(0)^2 L \bar J^2 |C|^2}, \tag{99}$$

$$r_a > \frac{2}{q_2(0)}\left(q_1(0) r_b p_1^2 + \frac{8}{\lambda_{\min}(Q)}|PB|^2\right), \tag{100}$$

$$\begin{aligned}
\mu_m < \min\Bigg\{ & \frac{1}{\sigma + \kappa_3 \bar D^2}\Bigg[\frac{7}{8}\lambda_{\min}(Q) \\
& - r_b\left(q_1(0)\bar D^2 - \frac{1}{2} q_1(0)^2 L \bar J^2 |C|^2\right)\Bigg], \\
& \frac{r_a\left(\frac{1}{2}\delta\underline{q_2} - \overline{c_4} - \frac{1}{2}\overline{q_2'}\right)}{\sigma}, \frac{r_b\left(\frac{1}{2}\underline{q_1}\delta - \overline{c_1} - \frac{1}{2} - \frac{1}{2}\overline{q_1'}\right)e^{-\delta L}}{\sigma}, \\
& \frac{\frac{1}{2} q_2(0) r_a - q_1(0) r_b p_1^2 - \frac{8}{\lambda_{\min}(Q)}|PB|^2}{\kappa_2 + \kappa_3 p_1^2},
\end{aligned} \tag{101}$$

$$\lambda_d \ge \max\left\{\frac{(\overline{q_2} + v_m) r_a e^{\delta L}}{2\mu_m}, 1\right\}, \tag{102}$$

$$\theta \le \frac{\sigma}{\lambda_d}, \tag{103}$$

where σ, η are free parameters. Applying the Young and Cauchy–Schwarz inequalities, recalling (58), we get

$$\begin{aligned}
& - r_a\int_0^{l(t)} e^{\delta x}\hat\eta(x,t)(\dot{\hat K} D_{\hat K(t)} X(t) + \dot{\hat K} R(x,t))dx \\
& \le \max_{i\in\{1,\dots,n\}}\{\gamma_{ci}\}\sqrt{n}\lambda_b(\zeta_p, \delta, r_a, r_b, \mu_m, \bar g_i)\left(|X(t)|^2 + \|\hat\eta\|^2\right)
\end{aligned} \tag{104}$$

where the positive constant $\lambda_b(\zeta_p, \delta, r_a, r_b, \mu_m, \bar g_i) > 0$ only depends on the plant parameters ζ_p and the choices of r_a, r_b, δ, μ_m and $\bar g_i$'s. Choosing parameters as (97)–(103) and inserting (104), the inequality (96) becomes

$$\begin{aligned}
\dot V(t) \le{}& \frac{1}{1+\Omega(t)-\mu_m m_d(t)}\Bigg[-\lambda_c(\zeta_p, \zeta_e, \delta, r_a, r_b, \mu_m, \bar g_i)\big(|X(t)|^2 \\
& + \hat\eta(0,t)^2 + \|\hat\eta(\cdot,t)\|^2 + \hat\alpha(l(t),t)^2 + \|\hat\alpha(\cdot,t)\|^2 + d(t)^2\big) \\
& + \mu_m\eta m_d(t) + \max_{i\in\{1,\dots,n\}}\{\gamma_{ci}\}\sqrt{n}\lambda_b(|X(t)|^2 + \|\hat\eta(\cdot,t)\|^2)\Bigg],
\end{aligned}$$

where the constant $\lambda_c(\zeta_p, \zeta_e, \delta, r_a, r_b, \mu_m, \bar g_i) > 0$ only depends on the plant parameters ζ_p, the design parameters $\bar g_i$'s in A_m, the event-triggering mechanism parameters ζ_e, and δ, r_a, r_b, μ_m in the adaptive law parameters. The coefficients γ_{ci} are independent of λ_b and λ_c. Choose $\max_{i\in\{1,\dots,n\}}\{\gamma_{ci}\}$ to satisfy

$$\max_{i\in\{1,\dots,n\}}\{\gamma_{ci}\} < \frac{\lambda_c(\zeta_p, \zeta_e, \delta, r_a, r_b, \mu_m, \bar g_i)}{\sqrt{n}\lambda_b(\zeta_p, \delta, r_a, r_b, \mu_m, \bar g_i)}. \tag{105}$$

Finally, we arrive at

$$\begin{aligned}
\dot V(t) \le{}& \frac{-\min\{\bar\lambda_c, \eta\}}{1+\Omega(t)}\Big(|X(t)|^2 + \hat\eta(0,t)^2 + \|\hat\eta(\cdot,t)\|^2 \\
& + d(t)^2 + \hat\alpha(l(t),t)^2 + \|\hat\alpha(\cdot,t)\|^2 + \mu_m|m_d(t)|\Big) \le 0,
\end{aligned} \tag{106}$$

where $\bar\lambda_c = \lambda_c - \max_{i\in\{1,\dots,n\}}\{\gamma_{ci}\}\sqrt{n}\lambda_b > 0$, and $\min\{\bar\lambda_c, \eta\}$ is related to the convergence rate of the closed-loop system.

Step 2. Boundedness analysis of $\frac{d}{dt}|X(t)|^2$, $\frac{d}{dt}\|\hat\eta(\cdot,t)\|^2$, $\frac{d}{dt}\|\hat\alpha(\cdot,t)\|^2$, *and* $\frac{d}{dt}|m_d(t)|$: According to (106) obtained in Step 1, we thus have $V(t) \le V(0)$, $\forall t \ge 0$. One easily gets that $|\tilde K(t)|^2$, $\|\hat\eta(\cdot,t)\|^2$, $\|\hat\alpha(\cdot,t)\|^2$, $|X(t)|^2$, $|m_d(t)|$ are uniformly bounded, and also $\Phi(t)$ is bounded according to (79). Recalling the invertibility of the backstepping transformations (37), (38), (50), the boundedness of the signals $\|\hat z(\cdot,t)\|$, $\|\hat w(\cdot,t)\|$, $|X(t)|$ is obtained. Therefore, $U(t)$ is bounded according to (69). It follows that $d(t)$ is bounded via (74). Taking the time derivative of $|X(t)|^2$, $\|\hat\alpha(\cdot,t)\|^2$, $\|\hat\eta(\cdot,t)\|^2$, and $|m_d(t)|$ along (52)–(56), (78), we obtain

$$\frac{d}{dt}|\hat X(t)|^2 = 2X^T(t)(A_m X(t) + B\hat\eta(0,t) - B\tilde K X(t)), \tag{107}$$

$$\begin{aligned}
\frac{d}{dt}\|\hat\eta(\cdot,t)\|^2 = {}& (q_2(l(t)) + \dot l(t))d(t)^2 - q_2(0)\hat\eta(0,t)^2 \\
& - \int_0^{l(t)}(q_2'(x) - 2c_4(x))\hat\eta(x,t)^2 dx \\
& + 2\int_0^{l(t)}\hat\eta(x,t)\Big[D(x;\hat K(t))B\tilde K(t) \\
& - \dot{\hat K}(t) D_{\hat K(t)}(x;\hat K(t))X(t) - \dot{\hat K}(t) R(x,t)\Big]dx,
\end{aligned} \tag{108}$$

$$\frac{d}{dt}\|\hat\alpha(\cdot,t)\|^2 = -(q_1(l(t)) - \dot l(t))\hat\alpha(l(t),t)^2 + q_1(0)\hat\alpha(0,t)^2$$

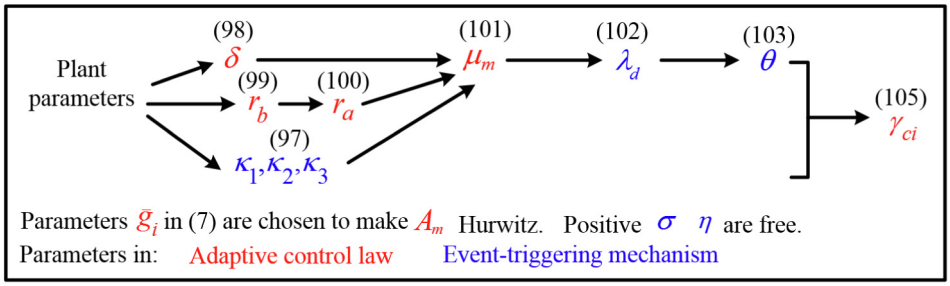

Fig. 2. A determination sequence of all design parameters under the cascaded conditions (97)–(103), (105) in the proposed adaptive event-triggered control system.

$$+\int_0^{l(t)}(q_1'(x)+2c_1(x))\hat{\alpha}(x,t)^2dx$$
$$-2\int_0^{l(t)}\hat{\alpha}(x,t)J(x,0)q_1(0)CX(t)dx, \tag{109}$$
$$\frac{d}{dt}|m_d(t)|=\eta m_d(t)-\lambda_d d(t)^2+\sigma\Phi(t)$$
$$+\kappa_1\hat{\alpha}(l(t),t)^2+\kappa_2\hat{\eta}(0,t)^2+\kappa_3\hat{\alpha}(0,t)^2, \tag{110}$$

where the fact $m_d(t)<0$ has been used in (110). Recalling the boundedness results proved above and (76), (74), (72), (69), we obtain the boundedness of $\hat{\eta}(l(t),t)$. We then have that $\hat{\eta}(0,t)$ is bounded as a result of the transport PDE (55), with recalling the boundedness of $\hat{K}$ in (123) in Appendix A. The signal $\hat{\alpha}(0,t)$ is bounded as well due to (53), and then $\hat{\alpha}(l(t),t)$ is bounded as a result of the transport PDE (54). Therefore, by applying the Young and Cauchy–Schwarz inequalities to (107)–(110), with the boundedness of $\dot{l}(t)$ in Assumption 3, we get that $\frac{d}{dt}|X(t)|^2$, $\frac{d}{dt}\|\hat{\eta}(\cdot,t)\|^2$, $\frac{d}{dt}\|\hat{\alpha}(\cdot,t)\|^2$, and $\frac{d}{dt}|m_d(t)|$ are uniformly bounded.

Finally, integrating (106) obtained in Step 1 from 0 to ∞, it follows that $|X(t)|^2$, $\|\hat{\alpha}(\cdot,t)\|^2$, $\|\hat{\eta}(\cdot,t)\|^2$, and $|m_d(t)|$ are integrable. Then using the results obtained in Steps 1 and 2, according to Barbalat's Lemma, we have that $|X(t)|^2$, $\|\hat{\alpha}(\cdot,t)\|^2$, $\|\hat{\eta}(\cdot,t)\|^2$, and $|m_d(t)|$ tend to zero as $t\to\infty$. ■

The following theorem establishes that, in the closed-loop system, no Zeno phenomenon takes place, namely that $\lim_{k\to\infty}t_k=+\infty$, and the states and the control signal are convergent to zero. The well-posedness of the event-based closed-loop system can be studied in a similar manner as in the proof of property 1) of Theorem 1 in Wang and Krstic (2021).

Theorem 1. *For all initial values $(z(\cdot,0),w(\cdot,0))\in L^2(0,L)$, $X(0)\in\mathbb{R}^n$, $(\hat{z}(\cdot,0),\hat{w}(\cdot,0))\in L^2(0,L)$, and $m_d(0)<0$, with the design parameters satisfying (97)–(103), (105), the closed-loop system, i.e., the plant (1)–(5) with the proposed observer-based adaptive event-triggered controller (91), which consists of the observer (14)–(17), the adaptive update law (63), (64), and the ETM (77), (78), has the following properties:*
1) There exits a positive constant $T_{\min}$ which only depends on the parameters of the plant and the choices of the design parameters such that $\min_{k\geq 0}\{t_{k+1}-t_k\}\geq T_{\min}$.
2) In the closed-loop system the states are asymptotically convergent to zero in the sense of

$$\lim_{t\to\infty}(|X(t)|^2+\|z(\cdot,t)\|^2+\|w(\cdot,t)\|^2$$
$$+\|\hat{z}(\cdot,t)\|^2+\|\hat{w}(\cdot,t)\|^2+|m_d(t)|)=0. \tag{111}$$

3) The adaptive event-triggered control signal is convergent to zero, i.e., $\lim_{t\to\infty}U_d(t)=0$.

Proof. 1) Recalling Lemma 4, property 1) is obtained.

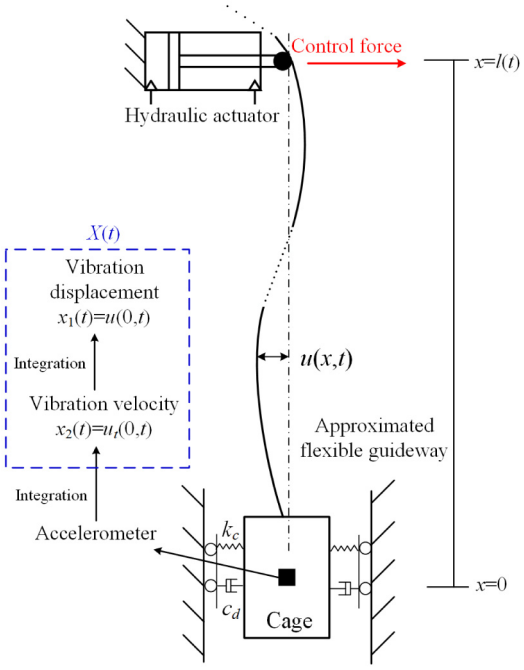

Fig. 3. Mining cable elevator with viscoelastic guideways.

2) Recalling the asymptotic stability result proved in Lemma 5, considering the invertibility and continuity of the backstepping transformations (37), (38), (50), we obtain the asymptotic convergence to zero of $\|\hat{z}(\cdot,t)\|^2+\|\hat{w}(\cdot,t)\|^2+|X(t)|^2+|m_d(t)|$. Recalling Lemma 1 and (18), applying the separation principle, property 2) is obtained.

3) Recalling (69) and property 2), we have that the continuous-in-time control signal $U(t)$ is asymptotically convergent to zero. According to the definition (72) and property 1), then property 3) is obtained. ■

Conditions on all the control parameters (97)–(103), (105) are cascaded rather than being mutually dependent. A sequence of determining these parameters is shown in Fig. 2. The choices of these parameters ensure the existence of a minimal dwell-time and the asymptotical stability of the closed-loop system. The optimal choices of these parameters are not studied in this paper.

7. Application in the flexible-guide mining cable elevator

7.1. Simulation model

The prominent characteristic of a mining cable elevator is captured as a load-moving cable system, where the control input and the payload are at the two boundaries of the cable whose length is time-varying, and its dynamics are

$$\rho u_{tt} = T(x)u_{xx}(x,t) + T'(x)u_x(x,t) - \bar{c}u_t(x,t), \tag{112}$$

$$M_c u_{tt}(0,t) = -k_c u(0,t) - c_d u_t(0,t) + T(0)u_x(0,t), \tag{113}$$

$$-T(l(t))u_x(l(t),t) = U(t) \tag{114}$$

where $u(x,t)$ denotes the lateral vibration displacements along the cable shown in Fig. 3, and $x \in [0, l(t)]$ are the positions along the cable in a moving coordinate system associated with the motion $l(t)$, whose origin is located at the cage. The function $T(x) = M_c g + x\rho g$ is the static tension along the cable and ρ is the linear density of the cable. The constant $\bar{c}$ is the material damping coefficient of the cable. The values of the physical parameters of the mining cable elevator tested in the simulation are shown in Table 1, which are taken from Wang, Pi, and Krstic (2018). The constants k_c, c_d are the unknown equivalent stiffness and damping coefficients of the viscoelastic guide. The modeling process of (112)–(114) refers to Canbolat, Dawson, Rahn, and Nagarkatti (1998). Through applying the Riemann transformations

$$z(x,t) = u_t(x,t) - \sqrt{\frac{T(x)}{\rho}}u_x(x,t), \tag{115}$$

$$w(x,t) = u_t(x,t) + \sqrt{\frac{T(x)}{\rho}}u_x(x,t), \tag{116}$$

and defining $X(t) = [x_1(t), x_2(t)]^T = [u(0,t), u_t(0,t)]^T$ which physically means the lateral displacement and velocity of the cage, (112)–(114) is converted into a 2×2 coupled transported PDE–ODE model in the form of (1)–(5) with the following coefficients:

$$q_1(x) = q_2(x) = \sqrt{\frac{T(x)}{\rho}}, c_1(x) = c_3(x) = \frac{-\bar{c}}{2\rho} - \frac{T'(x)}{4\sqrt{\rho T(x)}}, \tag{117}$$

$$c_2(x) = c_4(x) = \frac{-\bar{c}}{2\rho} + \frac{T'(x)}{4\sqrt{\rho T(x)}}, \ p_1 = -1, \tag{118}$$

$$A = \frac{1}{M_c}\begin{bmatrix} 0 & M_c \\ -k_c & -c_d - \sqrt{M_c \rho g} \end{bmatrix}, B = \begin{bmatrix} 0 \\ \sqrt{\frac{\rho g}{M_c}} \end{bmatrix}, \ C = [0, 2]. \tag{119}$$

For the lateral vibration model of the mining cable elevator (112)–(114) with the Riemann transformations (115), (116), the condition of the controlled boundary in (1)–(5) should have a simple augmentation, as follows:

$$w(l(t),t) = -\frac{2}{\sqrt{\rho T(l(t))}}U(t) + z(l(t),t). \tag{120}$$

The proximal reflection term $z(l(t),t)$ can be canceled at the drum (see Figure 1 (a) in Wang, Koga, et al. (2018)), so in the simulation, we consider the controlled boundary as (5), where the designed control input, based on (1)–(5) with the above coefficients (117)–(119), should be multiplied by $-\frac{\sqrt{\rho T(l(t))}}{2}$ to convert the input signal computed based on (5) into the control force at the head sheave in the mining cable elevator, i.e., into the control signal $U(t)$ in (120). In the practical mining cable elevator, $l(t)$ is obtained by the product of the radius and the angular displacement of the rotating drum driving the cable, where the angular displacement is measured by the angular displacement sensor at the drum.

Table 1
Physical parameters of the descending mining cable elevator.

Parameters (units)	Values
Initial length L_0 (m)	300
Final length (m)	2460
Cable linear density ρ (kg/m)	8. 1
Total hoisted mass M_c (kg)	15 000
Gravitational acceleration g (m/s^2)	9.8
Maximum hoisting velocities $\bar{v}_{\max}$ (m/s)	18
Total hoisting time t_f(s)	150
Cable material damping coefficient $\bar{c}$ (N s/m)	0.4

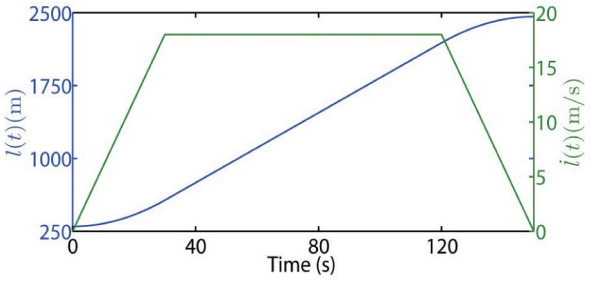

Fig. 4. Time-varying domain $l(t)$ and the according velocity $\dot{l}(t)$.

In the simulation, the unknown damping and stiffness coefficients of the flexible guide are set, respectively, as $c_d = 0.4$ and $k_c = 1000$. The target system matrix of the ODE is set as

$$A_m = \begin{pmatrix} 0 & 1 \\ -2.2 & -5.8 \end{pmatrix}. \tag{121}$$

The unknown target control parameters k_1, k_2 are sought online by the adaptive mechanism, to achieve the target system matrix A_m. The bounds of unknown control parameters k_1, k_2 in the adaptive estimates are defined as $[-50, 0]$, $[-100, 0]$. The time-varying cable length $l(t)$ and its changing rate $\dot{l}(t)$ are shown in Fig. 4. The maximum velocity of the moving boundary, i.e., the maximum hoisting velocity $\bar{v}_{\max} = 18$ m/s, satisfies the limit of the changing rate of the time-varying domain proposed in Assumption 3. The initial conditions of the plant (1)–(5) are defined as $w(x,0) = 0.2\sin(2\pi x/L_0)$, $z(x,0) = 0.4\sin(3\pi x/L_0 + \frac{\pi}{6})$, $x_2(0) = 0.5w(0,0) + 0.5z(0,0)$, $x_1(0) = 0.1$. The initial value $m_d(0)$ in the ETM is chosen as -0.03.

7.2. Simulation results

The design parameters in the proposed adaptive event-based control system are shown in Table 2. According to the system matrix, the input matrix in (119) and the target system matrix A_m in (121), we know that the ideal control parameters k_1, k_2 are -31.3,-78.2 respectively. Fig. 5 shows our adaptive design can online adjust the control parameters $\hat{k}_1(t), \hat{k}_2(t)$ to approach the ideal values. It often happens in the adaptive control that even though the estimates do not exactly arrive at their actual values, the state convergence is achieved in the closed-loop system, which can be seen shortly. The proposed adaptive event-based control input and the continuous-in-time adaptive control input are shown in Fig. 6. The internal dynamic variable $m_d(t)$ in the ETM is shown in Fig. 7. The PDE states used in the control law are from the observer (14)–(17), and the observer error is shown in Fig. 8, where we can see that observer errors at the midpoint of the time-varying spatial domain are convergent to zero after $t = 6.4s$.

Table 2
Parameters of the proposed adaptive event-based control system.

Parameters	Values
In adaptive update law	$\gamma_{c1} = 0.95$, $\gamma_{c2} = 0.46$, $\delta = 3$, $r_b = 0.06$, $r_a = 4$, $\mu_m = 0.00002$
In ETM	$\theta = 0.118$, $\eta = 41$, $\lambda_d = 1.3$, $\sigma = 0.5$, $\kappa_1 = \kappa_2 = \kappa_3 = 4$

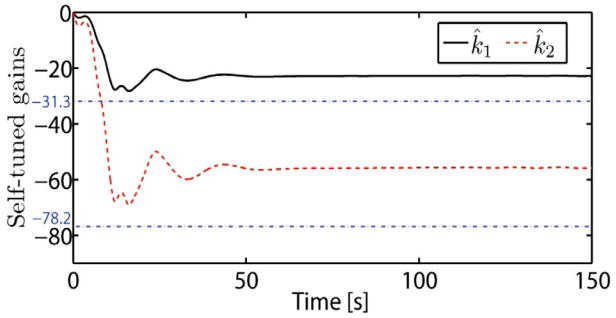

Fig. 5. Self-tuned control gains $\hat{k}_1, \hat{k}_2$, whose target values are $k_1 = -31.3, k_2 = -78.2$.

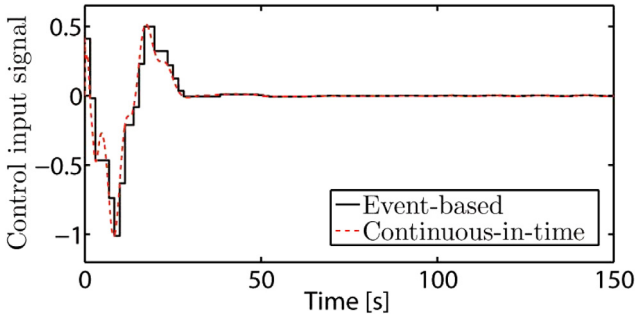

Fig. 6. Adaptive event-based control input and the continuous-in-time adaptive control input.

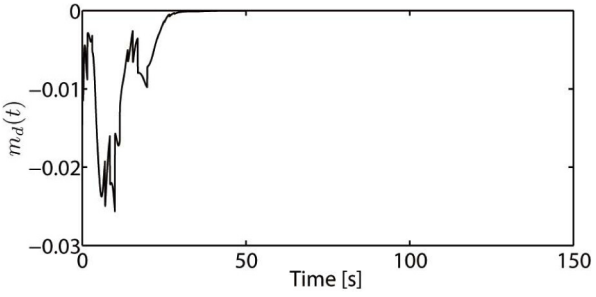

Fig. 7. Dynamic internal variable $m_d(t)$ in ETM.

The responses of the PDE states and the ODE state are shown in Figs. 9–12, where the proposed controller can quickly suppress to zero the oscillations appearing in the open-loop system. The fact that oscillation amplitude decreases in the open-loop system is due to the fact that material damping of the cable is considered in the simulation. Figs. 9 and 10 show that the PDE states at the midpoint of the time-varying spatial domain are reduced to zero. Figs. 11, 12 show that the responses of the ODE state $X(t) = [x_1(t), x_2(t)]^T$, which physically represent the displacement and velocity of the lateral vibrations of the cage moving along flexible guideways, are suppressed to zero under the proposed controller.

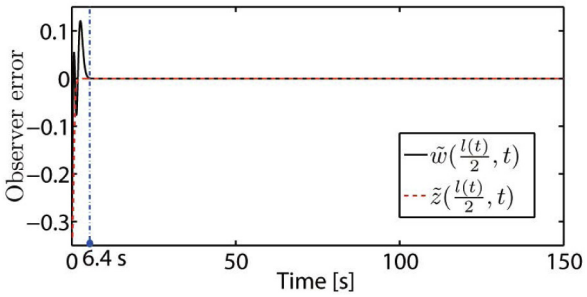

Fig. 8. Observer errors at the midpoint of the time-varying spatial domain.

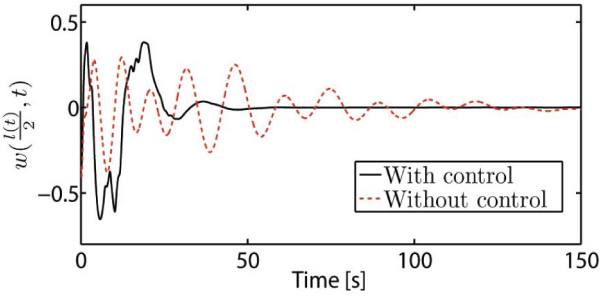

Fig. 9. Responses of $w\left(\frac{l(t)}{2}, t\right)$.

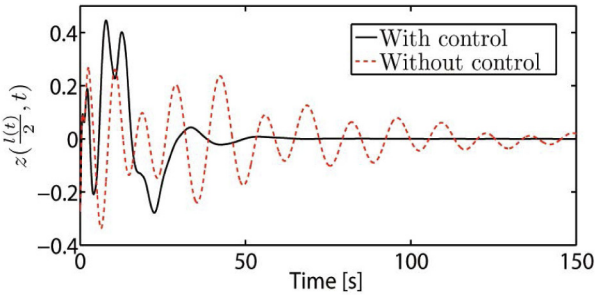

Fig. 10. Responses of $z\left(\frac{l(t)}{2}, t\right)$.

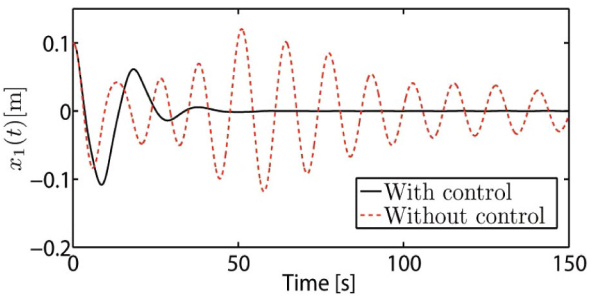

Fig. 11. Responses of $x_1(t)$.

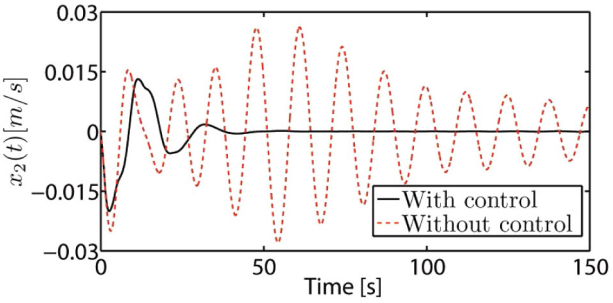

Fig. 12. Responses of $x_2(t)$.

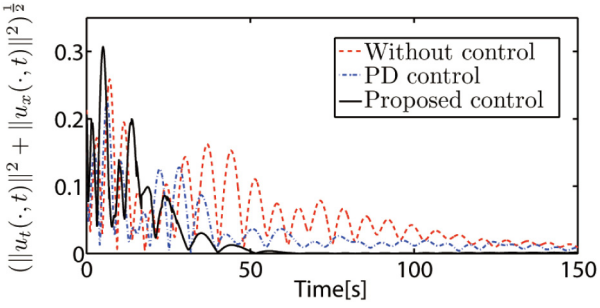

Fig. 13. Time evolution of the norm $(\|u_t(\cdot,t)\|^2+\|u_x(\cdot,t)\|^2)^{\frac{1}{2}}$ which physically reflects the vibration energy of the cable modeled by (112)–(114).

Representing the responses of $z(x,t)$, $w(x,t)$ in the original cable model (112)–(114) using (115), (116) as the norm $(\|u_t(\cdot,t)\|^2+\|u_x(\cdot,t)\|^2)^{\frac{1}{2}}$, which physically represents the vibration energy of the cable, a comparison of the performance of the proposed controller with the performance of a traditional PD controller $U_{pd}(t)=2x_1(t)+1.2x_2(t)$, where the PD parameters are chosen by trial and error over many tests, is shown in Fig. 13. From the comparison we observe that both controllers reduce the vibrations compared with the result without control. Even though the vibration energy under the proposed controller is larger at the beginning, which is due to the fact that the self-tuned control gains $\hat{k}_1, \hat{k}_2$ start to search for the target values from bad initial values of zero (see Fig. 5), the proposed controller reduces the vibration energy to a much smaller range around zero as time goes on.

8. Conclusion and future work

We propose an observer-based adaptive event-triggered boundary control of 2×2 coupled hyperbolic PDEs with spatially-varying coefficients and on a time-varying domain, whose uncontrolled boundary is coupled by a highly uncertain ODE. The control parameters can be self-tuned online to adjust the ODE system matrix with a high uncertainty, to a given target system matrix in the closed-loop system. The absence of a Zeno behavior and the asymptotic stability of the closed-loop system are proved. In numerical simulation, the proposed controller is applied in a mining cable elevator, which is representative of the load-moving cable systems, to suppress lateral vibrations during driving a cage moving along flexible guideways. In future work, the hydraulic actuator dynamics and external disturbances which often appear in practice will be incorporated into the control design. The optimal choices of the design parameters will also be studied.

Appendix A. Proof of Lemma 2

The following notation is used: $\bar{M}_{l(t)}(l(t),x;\hat{K}(t))=\frac{\partial \bar{M}(l(t),x;\hat{K}(t))}{\partial l(t)}$. Because of $\dot{U}_d=0$ for $t\in(t_k,t_{k+1})$, recalling (74), taking the time derivative along (13)–(17), we obtain

$$
\begin{aligned}
\dot{d}(t)^2=\dot{U}(t)^2=&\Big[\big(\dot{l}(t)-q_1(l(t))\big)\bar{M}(l(t),l(t),\hat{K}(t))\hat{z}(l(t),t)\\
&+\bar{M}(l(t),0;\hat{K}(t))q_1(0)\hat{z}(0,t)\\
&+\big(q_2(l(t))+\dot{l}(t)\big)\bar{N}(l(t),l(t),\hat{K}(t))\hat{w}(l(t),t)\\
&+\Big(D(l(t);\hat{K}(t))B-\bar{N}(l(t),0;\hat{K}(t))q_2(0)\Big)\hat{w}(0,t)\\
&+\Big(\dot{\hat{K}}(t)D_{\hat{K}(t)}(l(t);\hat{K}(t))+\dot{l}(t)D'(l(t);\hat{K}(t))+D(l(t);\hat{K}(t))A\Big)X(t)\\
&+\int_0^{l(t)}\Big((\bar{M}(l(t),x;\hat{K}(t))q_1(x))'+\bar{M}(l(t),x;\hat{K}(t))c_1(x)\\
&+\bar{N}(l(t),x;\hat{K}(t))c_3(x)+\dot{l}(t)\bar{M}_{l(t)}(l(t),x;\hat{K}(t))\\
&+\dot{\hat{K}}(t)\bar{M}_{\hat{K}(t)}(l(t),x;\hat{K}(t))\Big)\hat{z}(x,t)dx\\
&+\int_0^{l(t)}\Big(\bar{N}(l(t),x;\hat{K}(t))c_4(x)-(\bar{N}(l(t),x;\hat{K}(t))q_2(x))'\\
&+\dot{\hat{K}}(t)\bar{N}_{\hat{K}(t)}(l(t),x;\hat{K}(t))+\bar{M}(l(t),x;\hat{K}(t))c_2(x)\\
&+\dot{l}(t)\bar{N}_{l(t)}(x,l(t),\hat{K}(t))\Big)\hat{w}(x,t)dx\Big]^2\\
\le&\lambda_0(\zeta_p,\bar{g}_i)\big[\hat{w}(l(t),t)^2+\hat{z}(l(t),t)^2+\hat{w}(0,t)^2+\hat{z}(0,t)^2\\
&+m_3(\zeta_p,\zeta_a,\bar{g}_i)\|\hat{z}(\cdot,t)\|^2+m_3(\zeta_p,\zeta_a,\bar{g}_i)\|\hat{w}(\cdot,t)\|^2\\
&+m_3(\zeta_p,\zeta_a,\bar{g}_i)|X(t)|^2\big],
\end{aligned}
\tag{122}
$$

$t\in(t_k,t_{k+1})$, for some positive λ_0, which depends only on the plant parameters ζ_p and design parameters $\bar{g}_i$'s (the bounds of all kernels depend on the plant parameters ζ_p, and the bounds of $\hat{K}(t)$ depend on the bounds of the unknown parameters g_i's in A and the design parameters $\bar{g}_i$'s in A_m, as mentioned in Section 2). According to (63), (64), we know that

$$
\Big|\dot{\hat{K}}(t)\Big|^2\le m_3(\zeta_p,\zeta_a,\bar{g}_i) \tag{123}
$$

where m_3 is a positive constant dependent only on the plant parameters ζ_p, the adaptive law parameters ζ_a, and the design parameters $\bar{g}_i$'s in A_m. (In this paper a constant followed by $(\cdot)$ denotes that a constant that depends only on the parameters in the parentheses, as in (123).) Recalling the invertibility of the backstepping transformations $(\hat{z},\hat{w},X(t))\leftrightarrow(\hat{\alpha},\hat{\eta},X(t))$, inserting (76), then (81) is obtained. The proof is complete.

Appendix B. Proof of Lemma 3

According to (77), events are triggered to guarantee,

$$
d(t)^2\le\theta\Phi(t)-m_d(t). \tag{124}
$$

Inserting (124) into (78), one obtains

$$
\begin{aligned}
\dot{m}_d(t)\le&-(\eta+\lambda_d)m_d(t)+(\lambda_d\theta-\sigma)\Phi(t)-\kappa_1\hat{\alpha}(l(t),t)^2\\
&-\kappa_2\hat{\eta}(0,t)^2-\kappa_3\hat{\alpha}(0,t)^2\\
\le&-(\eta+\lambda_d)m_d(t)-\kappa_1\hat{\alpha}(l(t),t)^2\\
&-\kappa_2\hat{\eta}(0,t)^2-\kappa_3\hat{\alpha}(0,t)^2,\quad t\ge0
\end{aligned}
\tag{125}
$$

with using (82). Hence, by $m_d(0)<0$, we conclude that $m_d(t)<0$. The proof is complete.

Appendix C. Calculation of (87)

Taking the derivative of (83), using Lemma 2, and inserting the following inequality

$$-\dot{\Phi}(t) \leq \mu_0(\zeta_p,\zeta_a,\bar{g}_i)\Phi(t) + \lambda_p(\zeta_p)[\hat{\alpha}(l(t),t)^2 + \hat{\eta}(0,t)^2 + d(t)^2 + \hat{\alpha}(0,t)^2] \tag{126}$$

which is obtained by taking the derivative of $\Phi(t)$ along (52)–(56) for all $t \in [t^*, t_{k+1}]$ and recalling the boundedness of $\tilde{K}(t)$ (specifically, $|\tilde{K}(t)| \leq \sqrt{n} \times \max_{i\in\{1,\dots,n\}}(|\bar{k}_i - \underline{k}_i|)$) and the bound on $\dot{\hat{K}}(t)$ in (123), where the constant $\mu_0(\zeta_p,\zeta_a,\bar{g}_i) > 0$ in (126) only depends on the plant parameters ζ_p, adaptive law parameters ζ_a, and the design parameters $\bar{g}_i$'s, and where the constant $\lambda_p(\zeta_p) > 0$ in the same inequality only depends on the plant parameters ζ_p, we get

$$\begin{aligned}
\dot{\psi}(t) =& \frac{(2d(t)\dot{d}(t) + \frac{1}{2}\dot{m}_d(t))}{\theta\Phi(t) - \frac{1}{2}m_d(t)} - \frac{(\theta\dot{\Phi}(t) - \frac{1}{2}\dot{m}_d(t))}{\theta\Phi(t) - \frac{1}{2}m_d(t)}\psi(t) \\
\leq& \frac{1}{\theta\Phi(t) - \frac{1}{2}m_d(t)}\Bigg[\lambda_a\Big(d(t)^2 + \hat{\alpha}(l(t),t)^2 + \hat{\eta}(0,t)^2 \\
&+ \hat{\alpha}(0,t)^2 + m_3(\zeta_p,\zeta_a,\bar{g}_i)\|\hat{\alpha}(\cdot,t)\|^2 + m_3(\zeta_p,\zeta_a,\bar{g}_i)\|\hat{\eta}(\cdot,t)\|^2 \\
&+ m_3(\zeta_p,\zeta_a,\bar{g}_i)|X(t)|^2\Big) + d(t)^2 + \frac{1}{2}\dot{m}_d(t)\Bigg] \\
&- \frac{1}{\theta\Phi(t) - \frac{1}{2}m_d(t)}\Bigg[\theta\Big(-\mu_0(\zeta_p,\zeta_a,\bar{g}_i)\Phi(t) - \lambda_p\hat{\alpha}(l(t),t)^2 \\
&- \lambda_p\hat{\eta}(0,t)^2 - \lambda_p d(t)^2 - \lambda_p\hat{\alpha}(0,t)^2\Big) - \frac{1}{2}\dot{m}_d(t)\Bigg]\psi(t).
\end{aligned}$$

Inserting (78) to rewrite $\dot{m}_d(t)$, recalling (79), applying (84)–(86), we obtain that

$$\begin{aligned}
\dot{\psi}(t) \leq& \frac{1}{\theta\Phi(t) - \frac{1}{2}m_d(t)}\Bigg[\Big(\lambda_a + 1 + \frac{1}{2}\lambda_d\Big)d(t)^2 \\
&+ \lambda_a(\zeta_p,\bar{g}_i)m_3(\zeta_p,\zeta_a,\bar{g}_i)\Phi(t) - \frac{1}{2}\eta m_d(t)\Bigg] \\
&- \frac{1}{\theta\Phi(t) - \frac{1}{2}m_d(t)}\Bigg[-\Big(\theta\mu_0(\zeta_p,\zeta_a,\bar{g}_i) - \frac{1}{2}\sigma\Big)\Phi(t) \\
&- \Big(\theta\lambda_p + \frac{1}{2}\lambda_d\Big)d(t)^2 + \frac{1}{2}\eta m_d(t)\Bigg]\psi(t).
\end{aligned} \tag{127}$$

Applying, in (127), the following inequalities $-\frac{\frac{1}{2}\eta m_d(t)}{\theta\Phi(t)-\frac{1}{2}m_d(t)} \leq -\frac{\frac{1}{2}\eta m_d(t)}{-\frac{1}{2}m_d(t)} = \eta$, $\frac{\Phi(t)}{\theta\Phi(t)-\frac{1}{2}m_d(t)} \leq \frac{\Phi(t)}{\theta\Phi(t)} = \frac{1}{\theta}$, $\frac{d(t)^2}{\theta\Phi(t)-\frac{1}{2}m_d(t)} = \frac{d(t)^2+\frac{1}{2}m_d(t)-\frac{1}{2}m_d(t)}{\theta\Phi(t)-\frac{1}{2}m_d(t)} \leq \psi(t) + 1$, which hold because of $m_d(t) < 0$, then (87) is obtained.

Appendix D. Calculation of (96)

Taking the derivative of (92) along (52)–(55), employing (66), (67), (76), (78), and applying $\dot{\tilde{K}}(t) = -\dot{\hat{K}}(t)$, we obtain

$$\begin{aligned}
\dot{V}(t) =& \frac{1}{1 + \Omega(t) - \mu_m m_d(t)}\Bigg[-X^T(t)QX(t) + 2X^T PB\hat{\eta}(0,t) \\
&+ \frac{\dot{l}(t)}{2}r_b e^{-\delta l(t)}\hat{\alpha}(l(t),t)^2 + \frac{1}{2}(q_2(l(t)) + \dot{l}(t))r_a e^{\delta l(t)}\hat{\eta}(l(t),t)^2 \\
&- \frac{1}{2}q_2(0)r_a\hat{\eta}(0,t)^2 - \frac{1}{2}\delta r_a\int_0^{l(t)} e^{\delta x}q_2(x)\hat{\eta}(x,t)^2dx \\
&- \frac{1}{2}r_a\int_0^{l(t)} e^{\delta x}q_2'(x)\hat{\eta}(x,t)^2dx + r_a\int_0^{l(t)} c_4(x)e^{\delta x}\hat{\eta}(x,t)^2dx \\
&- \frac{1}{2}q_1(l(t))r_b e^{-\delta l(t)}\hat{\alpha}(l(t),t)^2 + \frac{1}{2}q_1(0)r_b\hat{\alpha}(0,t)^2 \\
&- \frac{1}{2}\delta r_b\int_0^{l(t)} e^{-\delta x}q_1(x)\hat{\alpha}(x,t)^2dx \\
&+ \frac{1}{2}r_b\int_0^{l(t)} e^{-\delta x}q_1'(x)\hat{\alpha}(x,t)^2dx + r_b\int_0^{l(t)} c_1(x)e^{-\delta x}\hat{\alpha}(x,t)^2dx \\
&- r_a\int_0^{l(t)} e^{\delta x}\hat{\eta}(x,t)\Big(\dot{\hat{K}}(t)D_{\hat{K}(t)}X(t) + \dot{\hat{K}}R(x,t)\Big)dx \\
&- r_b\int_0^{l(t)} e^{-\delta x}\hat{\alpha}(x,t)J(x,0)q_1(0)CX(t)dx \\
&+ \mu_m\eta m_d(t) - \mu_m\lambda_d d(t)^2 + \mu_m\sigma\Phi(t) \\
&+ \mu_m\kappa_1\hat{\alpha}(l(t),t)^2 + \mu_m\kappa_2\hat{\eta}(0,t)^2 + \mu_m\kappa_3\hat{\alpha}(0,t)^2\Bigg] \\
&- \tilde{K}(t)\Bigg[\Gamma_c^{-1}\dot{\hat{K}}(t)^T + \frac{1}{1 + \Omega(t) - \mu_m m_d(t)}\times\Bigg(2X(t)B^T PX(t) \\
&- r_a\int_0^{l(t)} e^{\delta x}\hat{\eta}(x,t)X(t)B^T D(x;\hat{K}(t))^T dx\Bigg)\Bigg].
\end{aligned} \tag{128}$$

Inserting the adaptive laws (63), (64) into (128), recalling (53), (76), and (79), applying the Young and Cauchy–Schwarz inequalities, (96) is obtained.

References

Anfinsen, H., & Aamo, O. M. (2017). Adaptive output-feedback stabilization of linear 2 × 2 hyperbolic systems using anti-collocated sensing and control. *Systems & Control Letters*, *104*, 86–94.

Anfinsen, H., & Aamo, O. M. (2018). Adaptive control of linear 2 × 2 hyperbolic systems. *Automatica*, *87*, 69–82.

Anfinsen, H., & Aamo, O. M. (2019). *Adaptive control of hyperbolic PDEs*. Springer.

Auriol, J., Aarsnes, U. J. F., Martin, P., & Di Meglio, F. (2018). Delay-robust control design for two heterodirectional linear coupled hyperbolic PDEs. *IEEE Transactions on Automatic Control*, *63*(10), 3551–3557.

Canbolat, H., Dawson, D., Rahn, C., & Nagarkatti, S. (1998). Adaptive boundary control of out-of-plane cable vibration. *Journal of Applied Mechanics*, *65*, 963–969.

Coron, J. M., Vazquez, R., Krstic, M., & Bastin, G. (2013). Local exponential H^2 stabilization of a 2 × 2 quasilinear hyperbolic system using backstepping. *SIAM Journal on Control and Optimization*, *51*(3), 2005–2035.

Davo, M. A., Bresch-Pietri, D., Prieur, C., & Di Meglio, F. (2018). Stability analysis of a 2 × 2 linear hyperbolic system with a sampled-data controller via backstepping method and looped-functionals. *IEEE Transactions on Automatic Control*, *64*(4), 1718–1725.

Deutscher, J. (2017a). Finite-time output regulation for linear 2 × 2 hyperbolic systems using backstepping. *Automatica*, *75*, 54–62.

Deutscher, J. (2017b). Output regulation for general linear heterodirectional hyperbolic systems with spatially-varying coefficients. *Automatica*, *85*, 34–42.

Di Meglio, F., Bribiesca, F., Hu, L., & Krstic, M. (2018). Stabilization of coupled linear heterodirectional hyperbolic PDE-ODE systems. *Automatica*, *87*, 281–289.

Espitia, N. (2020). Observer-based event-triggered boundary control of a linear 2 × 2 hyperbolic systems. *Systems & Control Letters*, *138*, Article 104668.

Espitia, N., Girard, A., Marchand, N., & Prieur, C. (2016a). Event-based stabilization of linear systems of conservation laws using a dynamic triggering condition. In *Proc. 10th IFAC symp. nonlinear control syst. (vol. 49)* (pp. 362–367). Monterey, CA, USA.

Espitia, N., Girard, A., Marchand, N., & Prieur, C. (2016b). Event-based control of linear hyperbolic systems of conservation laws. *Automatica*, *70*, 275–287.

Espitia, N., Girard, A., Marchand, N., & Prieur, C. (2018). Event-based boundary control of a linear 2 × 2 hyperbolic system via backstepping approach. *IEEE Transactions on Automatic Control*, *63*(8), 2686–2693.

Espitia, N., Karafyllis, I., & Krstic, M. (2021). Event-triggered boundary control of constant-parameter reaction–diffusion PDEs: A small-gain approach. *Automatica*, *128*, Article 109562.

Fridman, E., & Blighovsky, A. (2012). Robust sampled-data control of a class of semilinear parabolic systems. *Automatica*, *48*(5), 826–836.

Girard, A. (2015). Dynamic triggering mechanisms for event-triggered control. *IEEE Transactions on Automatic Control*, *60*(7), 1992–1997.

Gugat, M. (2007a). Optimal energy control in finite time by varying the length of the string. *SIAM Journal on Control and Optimization*, *46*, 1705–1725.

Gugat, M. (2007b). Optimal boundary feedback stabilization of a string with moving boundary. *IMA Journal of Mathematical Control and Information*, *25*, 111–121.

He, W., Meng, T., He, X., & Ge, S. S. (2018). Unified iterative learning control for flexible structures with input constraints. *Automatica*, *96*, 326–336.

He, W., Wang, T., He, X., Yang, L. J., & Kaynak, O. (2020). Dynamical modeling and boundary vibration control of a rigid-flexible wing system. *IEEE/ASME Transactions on Mechatronics*, http://dx.doi.org/10.1109/TMECH.2020.2987963.

He, W., Xiang, W.-J., He, X.-Y., & Li, G. (2020). Boundary vibration control of a floating wind turbine system with mooring lines. *Control Engineering Practice*, *101*, Article 104423.

Hu, L., Di Meglio, F., Vazquez, R., & Krstic, M. (2016). Control of homodirectional and general heterodirectional linear coupled hyperbolic PDEs. *IEEE Transactions on Automatic Control*, *61*(11), 3301–3314.

Kaczmarczyk, S., & Ostachowicz, W. (2003). Transient vibration phenomena in deep mine hoisting cables. Part 2: Numerical simulation of the dynamic response. *Journal of Sound and Vibration*, *262*(2), 245–289.

Karafyllis, I., Kontorinaki, M., & Krstic, M. (2019). Adaptive control by regulation-triggered batch least-squares. *IEEE Transactions on Automatic Control*, http://dx.doi.org/10.1109/TAC.2019.2933388.

Karafyllis, I., & Krstic, M. (2017). Sampled-data boundary feedback control of 1-D linear transport PDEs with non-local terms. *Systems & Control Letters*, *107*, 68–75.

Karafyllis, I., & Krstic, M. (2018a). Sampled-data boundary feedback control of 1-D parabolic PDEs. *Automatica*, *87*, 226–237.

Karafyllis, I., & Krstic, M. (2018b). Adaptive certainty-equivalence control with regulation-triggered finite-time least-squares identification. *IEEE Transactions on Automatic Control*, *63*, 3261–3275.

Karafyllis, I., Krstic, M., & Chrysafi, K. (2019). Adaptive boundary control of constant-parameter reaction–diffusion PDEs using regulation-triggered finite-time identification. *Automatica*, *103*, 166–179.

Liu, Z., He, X., Zhao, Z., Ahn, C. K., & Li, H. X. (2020). Vibration control for spatial aerial refueling hoses with bounded actuators. *IEEE Transactions on Industrial Electronics*, http://dx.doi.org/10.1109/TIE.2020.2984442.

Marchand, N., Durand, S., & Castellanos, J. F. G. (2013). A general formula for event-based stabilization of nonlinear systems. *IEEE Transactions on Automatic Control*, *58*(5), 1332–1337.

Selivanov, A., & Fridman, E. (2016). Distributed event-triggered control of diffusion semilinear PDEs. *Automatica*, *68*, 344–351.

Seuret, A., Prieur, C., & Marchand, N. (2014). Stability of non-linear systems by means of event-triggered sampling algorithms. *IMA Journal of Mathematical Control and Information*, *31*(3), 415–433.

Tabuada, P. (2007). Event-triggered real-time scheduling of stabilizing control tasks. *IEEE Transactions on Automatic Control*, *52*(9), 1680–1685.

Terumichi, Y., Ohtsuka, M., & Yoshizawa, M. (1997). Nonstationary vibrations of a string with time-varying length and a mass–spring system attached at the lower end. *Nonlinear Dynamics*, *12*, 39–55.

Vazquez, R., Krstic, M., & Coron, J. M. (2011). Backstepping boundary stabilization and state estimation of a 2 × 2 linear hyperbolic system. In *50th IEEE conference on decision and control and European control conference* (pp. 4937–4942).

Wang, J., Koga, S., Pi, Y., & Krstic, M. (2018). Axial vibration suppression in a PDE model of ascending mining cable elevator. *ASME Journal of Dynamic Systems, Measurement and Control*, *140*, Article 111003.

Wang, J., & Krstic, M. (2020). Vibration suppression for coupled wave PDEs in deep-sea construction. *IEEE Transactions on Control Systems Technology*, http://dx.doi.org/10.1109/TCST.2020.3009660.

Wang, J., & Krstic, M. (2021). Event-triggered output-feedback backstepping control of sandwich hyperbolic PDE systems. *IEEE Transactions on Automatic Control*, http://dx.doi.org/10.1109/TAC.2021.3050447.

Wang, J., Krstic, M., & Pi, Y. (2018). Control of a 2 × 2 coupled linear hyperbolic system sandwiched between two ODEs. *International Journal of Robust and Nonlinear Control*, *28*, 3987–4016.

Wang, J., Pi, Y., Hu, Y., & Gong, X. (2017). Modeling and dynamic behavior analysis of a coupled multi-cable double drum winding hoister with flexible guides. *Mechanism and Machine Theory*, *108*, 191–208.

Wang, J., Pi, Y., & Krstic, M. (2018). Balancing and suppression of oscillations of tension and cage in dual-cable mining elevators. *Automatica*, *98*, 223–238.

Wang, J., Tang, S. X., & Krstic, M. (2020a). Adaptive output-feedback control of torsional vibration in off-shore rotary oil drilling systems. *Automatica*, *111*, Article 108640.

Wang, J., Tang, S. X., & Krstic, M. (2020b). Lateral vibration suppression of a disturbed mining cable elevator with flexible guideways. In *59th IEEE conference on decision and control* (pp. 4436–4441).

Wang, J., Tang, S.-X., Pi, Y., & Krstic, M. (2018). Exponential anti-collocated regulation of the disturbed cage in a wave PDE-modeled ascending cable elevator. *Automatica*, *95*, 122–136.

Yao, Z., & El-Farra, N. H. (2013). Resource-aware model predictive control of spatially distributed processes using event-triggered communication. In *52nd IEEE conference on decision and control* (pp. 3726–3731).

Zhao, Z., Ahn, C. K., & Li, H. X. (2019). Boundary antidisturbance control of a spatially nonlinear flexible string system. *IEEE Transactions on Industrial Electronics*, *67*(6), 4846–4856.

Zhao, Z., Ahn, C. K., & Li, H. X. (2020). Dead zone compensation and adaptive vibration control of uncertain spatial flexible riser systems. *IEEE/ASME Transactions on Mechatronics*, *25*(3), 1398–1408.

Zhu, W. D., & Xu, G. Y. (2003). Vibration of elevator cables with small bending stiffness. *Journal of Sound and Vibration*, *263*, 679–699.

Ji Wang received the Ph.D. degree in Mechanical Engineering in 2018 from Chongqing University, Chongqing, China. From 2019, he is a Postdoctoral Scholar-Employee with the Department of Mechanical and Aerospace Engineering at University of California, San Diego, La Jolla, CA, USA. His research interests include modeling and control of distributed parameter systems, active disturbance rejection control, event-triggered control, and adaptive control, with applications in cable-operated mechanisms.

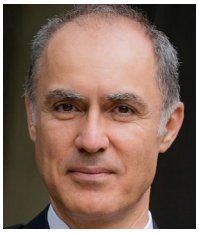

Miroslav Krstic is Distinguished Professor of Mechanical and Aerospace Engineering, holds the Alspach endowed chair, and is the founding director of the Cymer Center for Control Systems and Dynamics at UC San Diego. He also serves as Senior Associate Vice Chancellor for Research at UCSD. As a graduate student, Krstic won the UC Santa Barbara best dissertation award and student best paper awards at CDC and ACC. Krstic has been elected Fellow of seven scientific societies – IEEE, IFAC, ASME, SIAM, AAAS, IET (UK), and AIAA (Assoc. Fellow) – and as a foreign member of the Serbian Academy of Sciences and Arts and of the Academy of Engineering of Serbia. He has received the SIAM Reid Prize, ASME Oldenburger Medal, Nyquist Lecture Prize, Paynter Outstanding Investigator Award, Ragazzini Education Award, IFAC Nonlinear Control Systems Award, Chestnut textbook prize, Control Systems Society Distinguished Member Award, the PECASE, NSF Career, and ONR Young Investigator awards, the Schuck ('96 and '19) and Axelby paper prizes, and the first UCSD Research Award given to an engineer. Krstic has also been awarded the Springer Visiting Professorship at UC Berkeley, the Distinguished Visiting Fellowship of the Royal Academy of Engineering, the Invitation Fellowship of the Japan Society for the Promotion of Science, and four honorary professorships outside of the United States. He serves as Editor-in-Chief of Systems & Control Letters and has been serving as Senior Editor in Automatica and IEEE Transactions on Automatic Control, as editor of two Springer book series, and has served as Vice President for Technical Activities of the IEEE Control Systems Society and as chair of the IEEE CSS Fellow Committee. Krstic has coauthored fifteen books on adaptive, nonlinear, and stochastic control, extremum seeking, control of PDE systems including turbulent flows, and control of delay systems.